Unraveling the significance of the CCT/TRiC complex in medulloblastoma

Dissertation

zur Erlangung des akademischen Grades eines
Doktors der Medizin (Dr. med.)

an der

Medizinischen Fakultät der Universität Hamburg

vorgelegt von

Baolong Zheng

aus

Nei Mongol

2024

Betreuer:in / Gutachter:in der Dissertation: Prof. Dr. Julia Neumann

Gutachter:in der Dissertation: Prof. Dr. Julia Neumann, Prof. Dr. Ulrich Schüller

Vorsitz der Prüfungskommission: Prof. Dr. Ulrich Schüller

Mitglied der Prüfungskommission: Prof. Dr. Dr. Barbara M. Braunger

Mitglied der Prüfungskommission: Prof. Dr. Markus Glatzel

Datum der mündlichen Prüfung: 27.11.2025

Contents

1. Working hypothesis and questions

We hypothesize that (1) CCT/TRiC components drive cell proliferation and spreading in MB and (2) that a high abundance of CCT/TRiC components is related to therapy resistance in MB, and therefore correlates with a bad prognosis of patients. Finally, we ask which factors influence CCT/TRiC abundance patterns in MB. As CCT/TRiC components downregulation was particularly seen in WNT MB, we hypothesize that the Wnt/ ß-catenin signaling pathway may regulate upstream of the CCT/TRiC complex. Our results shall clarify whether the CCT/TRiC complex or its upstream regulators may represent new treatment targets that may be addressable in combination with chemotherapy.

2. Introduction

2.1 Medulloblastoma

Medulloblastoma is a type of childhood cerebellar malignant embryonal brain tumor first reported and named by Bailey and Cushing in 1925 (Bailey et al.,1926). Medulloblastoma is thought to arise from neural progenitor cell of the cerebellum and brain stem and may be located in the brain stem, or cerebellum (Schüller et al.,2008; , Gibson et al., 2010; , Smith et al., 2022) . During the embryonic period, an abnormal division and proliferation of these progenitor cells may cause medulloblastoma (Marino, 2005).

Medulloblastoma mainly occurs in children aged 5-7 years, with an average age of 14 years. Children under 12 years account for 69% of all patients with this tumor with a male-female ratio of 2:1 (Carta et al., 2020). Medulloblastoma accounts for 25%-30% of brain tumors in children and for more than 40% of posterior cranial fossa tumors in children. It is rare in adults, accounting for less than 1% of adult brain tumors (Fang et al., 2022).

Medulloblastoma is the most common malignant embryonal brain tumor in children. Medulloblastoma has a low degree of differentiation, grows rapidly, and has a short course of disease. The average time from onset to treatment is about 4 months, the shortest is 10 days, and the longest is no more than 1 year. Because medulloblastoma often occurs in the cerebellar vermis, patients often have symptoms of ataxia such as unstable gait (Raffel, 2004). If the tumor protrudes into the fourth ventricle, it may block the aqueduct upwards and the median foramen downwards, and may grow into the cerebellomedullary cistern, resulting in obstruction of cerebrospinal fluid circulation, causing hydrocephalus and increased intracranial pressure. Patients are prone to symptoms of meningeal irritation such as headache (79%), vomiting (82%), and papilledema (75%) (Ryzhova et al., 2013).

The tumor cells of medulloblastoma may spread along the subarachnoid space and may form metastases. Common sites for metastases are the spinal cord, especially the cauda equina, or more rarely the ventricles (Meister et al., 2022). In very care cases, medulloblastoma can spread to other parts of the body through the blood and forms extracranial metastasis in the

lungs, bones or lymph nodes (Varan et al., 2006). Metastases may occur after surgery (Rickert, 2003; Campbell et al., 1984) with the time for the occurrence of metastatic symptoms ranging from 8 months to 6 years after surgery, but mostly within 1 year after surgery (Mazloom et al., 2010).

The goal of treating medulloblastoma is to remove the tumor to the maximum extent possible while preserving neurological function as much as possible, and to reduce the risk of recurrence through radiotherapy and chemotherapy. Before treatment begins, a detailed diagnostic evaluation is first required. This includes: confirming the location, size, and morphology of the tumor through MRI or CT scans, and evaluating its impact on the surrounding brain tissue and cerebrospinal fluid pathways. Lumbar puncture can detect cancer cells in the cerebrospinal fluid and determine whether the tumor has spread. If medulloblastoma spreads through the cerebrospinal fluid, the scope of radiotherapy usually includes the entire brain and spinal cord, which is termed craniospinal irradiation (CSI) (Merchant et al., 2008). Commonly used chemotherapy drugs include cisplatin, vincristine or cyclophosphamide, and more, which aim to eliminate possible tiny residual tumor lesions. For high-risk patients, high-dose chemotherapy can be performed, followed by autologous stem cell transplantation to help bone marrow recovery (Choi, 2023). In recent years, methods of molecular characterization enabled a rapid progress in the subtyping of medulloblastomas based on genomic alterations, DNA-methylation, global RNA expression and protein abundance (Cavalli et al., 2017; Northcott et al., 2017; Sharma et al., 2019; Taylor et al., 2012; Godbole et al., 2024; Forget et al., 2018), which provides new possibilities for personalized treatment. Future treatments may rely more and more on molecular targeted therapy and immunotherapy, which are expected to reduce side effects while improving efficacy.

2.2 Medulloblastoma Molecular Subtypes

In 2006, Thompson et al. proposed that medulloblastoma can be grouped according to similar genomic expression profiles (Thompson et al., 2006). In 2010, researchers further defined genomic features based on genomic and transcriptomic changes and integrated molecular subdivision groups into patient demographics and clinical outcomes (Northcott et al., 2010; Hovestadt et al., 2020). The heterogeneity of medulloblastoma patients and the differences

in prognosis illustrate the limitations of the actual WHO grading in predicting prognostic value. Therefore, it is necessary to develop better criteria to evaluate the behavior of medulloblastoma and the effect of treatment.

In 2010, the World Health Organization (WHO) first divided medulloblastoma into four molecular subtypes by molecular markers: WNT subtype, SHH subtype, Group 3 subtype, and Group 4 subtype (Taylor et al., 2012). WNT and SHH subtypes induce tumors through gene mutations that lead to upregulation of the WNT and Sonic hedgehog (SHH) pathways, respectively. The potential genetic drivers of Group 3 and Group 4 subtypes are less uniform, so generic names are used temporarily (Cho et al., 2011; Northcott et al., 2011; Ellison et al., 2011). To account for the increasing significance of molecular characteristics, the current WHO classification of 2021 included molecular parameters for classification and grading of brain tumors, enhancing integrated diagnostics (Louis et al., 2021; Sturm et al., 2023).

Proteins as building blocks of the cell can represent direct therapy targets and hence proteins patterns of tumors may reveal distinct therapeutic vulnerabilities. Based on global protein patterns, six proteomic medulloblastoma subtypes were detected that were divided into two main categories: transcription/translation (pSHHt, pWNT, and pG3myc) and synaptic/immune processes (pSHHs, pG3, and pG4). Multi-omics analysis revealed differences in DNA methylome levels and N-glycosylation levels among the different medulloblastoma subtypes (Godbole et al., 2024). Certain protein and N-glycan structures may provide a new direction for the diagnosis and treatment of patients with medulloblastoma underlining the importance of a thorough molecular profiling. In the following the main types of medulloblastoma will be further introduced.

2.2.1 WNT subtype

WNT subtype medulloblastoma originates from embryonic brain stem progenitor cells (Gibson et al., 2010). It is named WNT subtype because of gene mutations that increase the activity of the WNT pathway (Helgager et al., 2020). Among all subtypes, it has the most consistent

genetic mutation pattern, and almost all tumors have classical histological features. The WNT subtype accounts for only 10% of all medulloblastomas and is the subtype with the smallest number of patients, but has the best prognosis. Patients are mainly adolescents, rarely infants, and there is no significant gender difference (Kool et al., 2012). The 5-year survival rate of adolescent patients exceeds 95%, which may be related to the fact that the WNT subtype rarely metastasizes and the fact that these tumors represent an incomplete blood-brain barrier, which enables chemotherapy drugs to accumulate in the tumor (Phoenix et al., 2016).

85%-90% of patients with the WNT subtype have activating mutations in exon 3 of the CTNNB1 gene, which is the most prominent feature of the WNT subtype. The CTNNB1 gene encodes the β-catenin protein. Mutated β-catenin protein accumulates in the cell nucleus (Rogers et al., 2009). Mutated β-catenin protein, as an important effector of the WNT signaling pathway, works together with the TCF-LEF family transcription factors to further constitutively activate downstream target genes, causing the occurrence of this subtype of medulloblastoma (Cadigan et al., 2012). Therefore, a CTNNB1 gene mutation and nuclear accumulation of the β-catenin protein using immunohistochemistry can be used as the molecular pathological diagnostic standard. Further, a specific criterium for this subtype is the loss of chromosome 6 (Clifford et al., 2006). However, chromosome 6 loss and/or CTNNB1 gene mutation does not apply to all WNT subtype patients. 10%-15% of WNT subtype medulloblastoma patients do not meet this diagnostic criterion (Waszak et al., 2018; Goschzik et al., 2022). Clifford et al. used the similarity network fusion method to identify two subtypes: WNTα and WNTβ. WNTα is mainly found in children, with 98% of patients having haploidy on chromosome 6; WNTβ is mainly represented in adolescents and adults, with 29% of patients having diploidy on chromosome 6 (Clifford et al., 2006).

2.2.2 SHH subtype

Sonic hedgehog (SHH) subtype medulloblastoma originates from the granule neuron precursors (GNPs) of the cerebellum and is often located in one unilateral hemisphere of the cerebellum (Hatten et al., 1995). It is named SHH subtype because of gene mutations that

increase the activity of the SHH pathway. This subtype accounts for about 30% of all medulloblastomas. The age of onset distribution of this subtype of medulloblastoma is bimodal. About 70% of medulloblastoma patients are under 3 years old or over 16 years old, with no significant gender difference (Rutkowski et al., 2010). The histopathology of SHH subtype comprises classic and desmoplastic/nodular patterns (DN) but is not specific. However, almost all medulloblastoma with extensive nodularity (MBEN) belong to the SHH subtype (Northcott et al., 2012). The prognosis is moderate, with a 5-year survival rate of 60% to 80% (Taylor et al., 2012; Louis et al., 2007). Compared with the WNT subtype, histological and molecular characteristics and clinical outcomes of SHH medulloblastoma show more variability.

In children, tumors often occur in the cerebellar vermis, while in adults, tumors are more common in the cerebellar hemispheres (Wefers et al., 2014; Ohli et al., 2015). This age tendency may be attributed to different tumor-initiating driver mutations. In the pediatric and adult (>16 years) patient cohorts, significant differences in genetic profiles are closely related to patient survival, and adult SHH subtype patients tend to have longer survival than pediatric patients (Wong et al., 2020). TP53 gene mutation may be the most important risk factor for poor prognosis in children with SHH subtype (Zhukova et al., 2013).

Studies have shown that SHH subtype medulloblastoma can be divided into different subtypes based on age. For example, Schwalbe et al. divided SHH subtypes into two categories: MBSHH-Infant (less than 4.3 years old) and MBSHH-Child (greater than or equal to 4.3 years old). Among them, MBSHH-Infant usually presents as DN type, rich in SUFU gene mutations, with a good prognosis and a 5-year overall survival rate of about 62%; while MBSHH-Child mostly presents as large cell/anaplastic (LC/A), accompanied by TP53, TERT gene mutations and MYCN, GLI2 gene amplification, and high DNA methylation levels, chromosome 9q loss and 9p gain, and a 5-year overall survival rate of about 58% (Schwalbe et al., 2017).

In addition, Robinson et al. divided SHH subtype medulloblastoma in children aged 5 years and younger into two categories based on differences in methylation types: iSHH-I and iSHH-II. The median age of iSHH-I is 2.0 years, the male-female ratio is 1.3:1, it is rich in SUFU gene mutations and chromosome 2 gain, the prognosis is poor, and the 5-year survival rate is 27.8%;

the median age of iSHH-II is also 2.0 years, the male-female ratio is 1:1.3, it is rich in SMO activating mutations and chromosome 9q loss, the prognosis is good, and the 5-year survival rate is 75.4% (Robinson et al., 2018).

Finally, Cavalli et al. identified four subtypes of SHHα, SHHβ, SHHγ and SHHδ through comprehensive cluster analysis: SHHα has the worst prognosis, accompanied by TP53 gene mutations, and is rich in MYCN, GLI2, YAP1 gene amplification and chromosome 9q, 10q and 17p loss; SHHβ is more common in infants and young children, usually accompanied by metastasis, and has a poor prognosis; SHHγ pathology is mostly MBEN, with a better prognosis; SHHδ is mainly composed of adults and is rich in TERT promoter mutations (Cavalli et al., 2017).

Based on proteome profiles two subtypes have been described, a synaptic SHH type (pSHHsyn) and a transcriptional/ translational subtype (pSHHt), however, their clinical significance still remains unknown (Godbole et al., 2024).

2.2.3 Group 3 medulloblastoma subtype

Group 3 medulloblastoma derives from progenitor cells of the rhombic lip (Smith et al., 2022) and is often located in the brainstem and fourth ventricle. It is prone to metastasis (Raybaud et al., 2015). This subtype accounts for about 25% of all subtypes, and the 5-year survival rate of patients is about 50%, which is the worst treatment effect among all subtypes. Patients of Group 3 subtype are almost all infants and young children, rarely adults, and the male-to-female ratio is 2:1 (Kool et al., 2012). The pathological type is mainly classical, but 40% of large cell/ anaplastic (LC/A) medulloblastomas also belong to this subtype. 17% of patients have high expression and amplification of the MYC gene, which is the most important feature of this type. At the same time, most patients are accompanied by an amplification of the non-coding RNA PVT1, which can assist in the overexpression of the MYC protein (Pitolli et al., 2023).

Studies have shown that enhancer hijacking occurs in 15%-20% of Group 3 medulloblastoma patients, leading to upregulation of the oncogenes GFI1 and GFI1B, which may be an important driver event for Group 3 subtype (Northcott et al., 2014). Amplification of

chromosomes 1q, 7, and 17q, deletion of 10q, 11q, 16q, and 17p, and the presence of isochromosome 17q (i17q) are the main cytogenetic manifestations of Group 3 subtype. At the same time, i17p can be used as an important marker for poor prognosis of the Group 3 subtype (Northcott et al., 2012; Shih et al., 2014). NPR3 protein can be used as a molecular pathological diagnostic criteria for Group 3 subtype medulloblastoma (Ntenti et al., 2023).

Schwalbe et al. divided Group 3 subtype medulloblastoma into two categories: MBGrp3-HR and MBGrp3-LR. MBGrp3-HR usually presents as LC/A type, characterized by MYC gene overexpression, GFI1 gene mutation, i17q abnormality, and a large number of methylated CpG sites. The 5-year overall survival rate of such patients is about 37%. In contrast, the pathological type of MBGrp3-LR is usually classical, more common in infants and young children, manifested by multiple chromosome deletions, with a relatively good prognosis and a 5-year survival rate of about 70% (Schwalbe et al., 2017).

In addition, Cavalli et al. identified three subtypes of Group 3 through comprehensive cluster analysis based on RNA expression and DNA methylation data: Group 3α, Group 3β, and Group 3γ. Group 3α is mainly distributed in infants and young children, often metastasizes, and has a relatively good prognosis; Group 3β rarely metastasizes, has a better prognosis, and has a high frequency of activation of *GFI1* and *GFI1B* proto-oncogenes, often accompanied by *OTX2* amplification; Group 3γ is most likely to metastasize (40%-50%) and has the worst prognosis of all subtypes, with a 5-year survival rate of less than 60%. It often has an 8q gain, is enriched in i17q, and has an increase in the copy number of the *MYC* gene (located at 8q24) (Cavalli et al., 2017).

2.2.4 Group 4 medulloblastoma subtype

Group 4 medulloblastoma may derive from progenitor cells of the rhombic lip (Smith et al., 2022; Robinson et al., 2018). The site of onset is similar to that of Group 3, usually in the fourth ventricle. Group 4 medulloblastoma is the most common subtype, accounting for 35%-40% of all medulloblastomas. The peak age of onset of this subtype is between 5 and 13 years. It is relatively rare in infants, and the male-female ratio is nearly 2:1 (Kijima et al., 2016). After standard treatment, the prognosis of patients is similar to that of the SHH subtype. 30-40% of

patients have leptomeningeal metastasis. Pathologically, the classic type is the most common. Studies have shown that follistatin-related protein 5 (FSTL5) is a biological marker for poor prognosis of Group 4 MB (Kijima et al., 2016). There are a large number of chromosomal aberrations in this subtype, and the most common structural change is i17q, accounting for about 80%. The most significant driving event of the Group 4 subtype is the activation and overexpression of the PRDM6 gene (Kumar et al., 2020). About 13% of Group 4 subtype patients have mutations in the KDM6A gene, which is located on the X chromosome and encodes a histone demethylase (H3K27) (Skowron et al., 2015). This X-chromosome-related mutation may lead to gender differences in patients with this subtype.

Schwalbe et al. divided the Group 4 subtype into two categories: MBGrp4-HR and MBGrp4-LR. MBGrp4-HR, the pathological type is mostly classic, and there is often amplification of PRDM6; MBGrp4-LR pathology is mostly classic, with obvious MYCN amplification, accompanied by amplification of chromosomes 7 and 17q and deletion of chromosomes 8 and 11, and the 5-year survival rate is about 80% (Schwalbe et al., 2017). Cavalli et al. identified three subtypes through comprehensive cluster analysis: Group 4α, Group 4β and Group 4γ. Group 4α showed increased amplification of MYCN, loss of chromosome 8p and increased amplification of chromosome 7q; Group 4β showed increased amplification of SNCAIP and i17q; Group 4γ showed increased amplification of CDK6 (Cavalli et al., 2017).

2.3 CCT/TRiC complex

Proteomic profiling of medulloblastoma has identified the components of the Chaperonin Containing TCP-1 (CCT) complex to be specifically upregulated in poor prognostic MYC activated Group 3 medulloblastoma. In contrast CCT components were downregulated in WNT medulloblastoma with rather good prognosis (Godbole et al., 2024). The significance of this complex and its components in medulloblastoma is however unknown.

The CCT complex is a complex multi-subunit protein complex whose activity may affect the occurrence and development of cancer. The structure of the CCT complex is composed of two ring-shaped parts stacked around a central cavity. Each ring is composed of 8 different subunits, which are encoded by CCT1-8 or CCTα-θ genes and arranged in a specific way (Leitner et al., 2012). The CCT complex can help about 10% of eukaryotic cell proteins fold.

Some key cellular proteins, such as cytoskeletal proteins, cell cycle regulators, and tumor signaling pathway-related proteins, can only be correctly folded with the assistance of the CCT complex (Yam et al., 2008).

The CCT complex plays a key role in maintaining intracellular protein homeostasis and the integrity of the overall proteome by folding microtubules (such as tubulins) and actin (such as actins) (Sternlicht et al., 1993). In addition, studies have shown that if the CCT complex binding site of the von Hippel-Lindau (VHL) is missing, VHL will misfold, thereby promoting tumor formation. Signal transducer and activator of transcription 3 (STAT3) regulates a variety of biological processes related to tumorigenesis, such as cell survival, cell cycle progression, and angiogenesis. Studies have found that STAT3 needs to be correctly folded with the help of the CCT complex in order to function normally (Vallin et al., 2021).

Cell proliferation, migration and invasion are the main driving factors of tumor occurrence and progression, and these processes are accompanied by the interaction of CCT complex with its substrates such as actin, tubulin, VHL, PHD3, STAT3 and other proteins. Proteins such as p53 and Cdc20 need to bind to CCT complex to regulate cell cycle signaling pathways, thereby affecting tumor occurrence and development (Trinidad et al., 2013; Camasses et al., 2003). Other cell cycle-related proteins such as Cyclin D, Cyclin E and p21 can interact with CCT complex to lead to tumor development, proliferation and metastasis (Meng et al., 2021; Yokota et al., 1999). Studies have found that blocking the activity of CCT complex can lead to significant changes in cell morphology and cell cycle arrest. Tumor suppressors such as p53 and VHL can bind to CCT complex to promote tumor progression. CCT complex can also work with p21-activated protein kinase 4 (PAK4) and gelsolin to act on actin, thereby promoting cell migration (Zhao et al., 2017).

Studies have shown that the CCT complex not only functions as a whole, but its individual subunits can also participate in the proliferation and migration of tumor cells individually. In many types of cancers, such as lung cancer, colorectal cancer, pancreatic cancer and glioma, multiple subunits of the CCT complex show high expression, which is closely related to the occurrence, development and poor prognosis of these cancers. In particular, the three subunits CCT-3, CCT6 and CCT-8 can interact with more substrates, while CCT-2 and CCT-8 are

more easily separated from the CCT complex, so these subunits may play a greater role in maintaining cancer cell protein balance and promoting cancer progression (Spiess et al., 2015). At present, although the specific mechanism of action of CCT subunits in tumors is not well understood, and the related oncogenic signaling pathways are still under study, it is certain that CCT subunits are essential for the survival and proliferation of cancer cells. Further research on the functions and oncogenic mechanisms of CCT subunits will help develop new cancer diagnostics and treatments.

CCT-8 is located on chromosome 21q21.3 and is highly expressed in a variety of tumor tissues (Nomura et al., 1994). Patients with high expression of CCT-8 have a reduced overall survival rate. Studies have found that CCT-8 can interact with LASP1, inhibit WTp53 from entering the nucleus, antagonize WTp53-mediated cell cycle arrest and EMT transcription factor inhibition, and promote the proliferation, metastasis and invasion of colon cancer cells (Liao et al., 2021). In pancreatic cancer, CCT-8 in the blood can be used as a biomarker for pancreatic cancer invasion and metastasis and can assess the prognosis of pancreatic cancer patients (Liu et al., 2019). CCT-8 is an enriched protein in hepatocyte-derived exosomes and can be used as a potential diagnostic and prognostic serum biomarker for patients with primary liver cancer (Cho et al., 2021). CCT-8 accelerates the transition of G/S phase and promotes HCC cell proliferation by upregulating the expression levels of proliferating cell nuclear antigen (PCNA), cyclin E and cyclin-dependent kinases 2 (CDK2) in liver cancer cells (Liu et al., 2021). Studies have also found that CCT-8 can promote the transition of G1/S phase in non-Hodgkin's lymphoma cells, thereby accelerating tumor cell proliferation (Yin et al., 2016).

It has been reported that silencing CCT-8 in U87MG and U251MG glioma cells will inhibit the G1/S phase process and thus affect the entire cell cycle process to inhibit the carcinogenicity of tumor cells, and can also significantly reduce the migration and invasion ability of tumor cells (Qiu et al., 2015).

In this work, we aimed to unravel the functional significance of the CCT complex in medulloblastoma.

3. Material and Methods

3.1 Material

3.1.1 Consumables and Equipment

Fig. 1: Consumables. All consumables used and their manufacturers (company name, location) are listed.

Consumable	Company
96-well microtiter plate	Promega Corporation, Madison, USA
Aluminium foil	Sarstedt AG & Co., Nümbrecht, DE
Disposable serological pipette	Sarstedt AG & Co., Nümbrecht, DE
Cell culture plate	Sarstedt AG & Co., Nümbrecht, DE
Disposable bag	Sarstedt AG & Co., Nümbrecht, DE
Sterile gloves	Thermo Fisher Scientific Inc., Waltham, USA
Reagent bottle	SCHOTT AG, Mainz, DE
Colour coded insert	Sarstedt AG & Co., Nümbrecht, DE
Cell scraper	Sarstedt AG & Co., Nümbrecht, DE
Glass disposable counting chamber	Anvajo GmbH, Dresden, DE
Cover glass	SCHOTT AG, Mainz, DE
Parafilm	Bemis Company, Inc., Neenah, USA
Petri dish	Sarstedt AG & Co., Nümbrecht, DE
Tweezer	Servoprax GmbH, Wesel, DE
Pipette tip	STARLAB GmbH, Hamburg, DE
PCR tube	Eppendorf AG, Hamburg, DE
Eppendorf tube	Eppendorf AG, Hamburg, DE
Syringe	B. Braun Melsungen AG, Melsungen, DE
Western blotting box	BioRad Laboratories, München, DE
White 96 well plate	Thermo Fisher Scientific Inc., Waltham, USA
Filter paper	BioRad Laboratories, München, DE
Cell culture flask	STARLAB GmbH, Hamburg, DE
PVDF membrane	BioRad Laboratories, München, DE
CryoPure Tube	Sarstedt AG & Co., Nümbrecht, DE
PH test paper	BioRad Laboratories, München, DE
Sponge	BioRad Laboratories, München, DE
Falcon tube	Sarstedt AG & Co., Nümbrecht, DE
Scissor	BioRad Laboratories, München, DE

Lab spoon	BioRad Laboratories, München, DE
Sterilization indicator tape	3M Deutschland GmbH, Neuss, DE

Fig. 2: Equipment. All equipment used are listed and their manufacturers (company name, location) are listed.

Equipment	Company
8 canal pipette	Eppendorf AG, Hamburg, DE
Clean bench	Thermo Fisher Scientific Inc., Waltham, USA
Electronic Pipette	Eppendorf AG, Hamburg, DE
Image scanner microscope	Olympus Corporation, Tokyo, JP
Hand counter	Greiner Bio-One International GmbH, Kremsmünster, AT
Incubator	neoLab Migge GmbH, Heidelberg, DE
Cell Counting Chamber	MUHWA Ltd., Shanghai, CN
Cooled centrifuge	Braun Melsungen AG, Melsungen, DE
Magnetic rack	Thermo Fisher Scientific Inc., Waltham, USA
Magnetic stirrer	Braun Melsungen AG, Melsungen, DE
Massenspektrometer	Thermo Fisher Scientific Inc., Waltham, USA
Pipette	Eppendorf AG, Hamburg, DE
Printer	Hewlett-Packard Company, USA
Microscope	Olympus Corporation, Tokyo, JP
Microplate reader	Promega Corporation, Madison, USA
NanoEase	Waters GmbH, Eschborn, DE
nano-UHPLC	Thermo Fisher Scientific Inc., Waltham, USA
Nano Viper	Thermo Fisher Scientific Inc., Waltham, USA
Electrophoresis power supply	Biometra GmbH, Göttingen, DE
Fume hood	Thermo Fisher Scientific Inc., Waltham, USA
Freezer	Liebherr CO., Ltd., Shanghai, CN
Fridge	Liebherr CO., Ltd., Shanghai, CN
funnel	BRAND GMBH + CO KG, Frankfurt am Main, DE
graduated cylinder	BRAND GMBH + CO KG, Frankfurt am Main, DE
Sharps disposal container	Herli Medical BV, Kontich, BE
Shelf	Herli Medical BV, Kontich, BE
Spectrophotometer	NanoDrop Technologies Inc., Wilmington, USA
Table centrifuge	B. Braun Melsungen AG, Melsungen, DE
thermometer	Thermo Fisher Scientific Inc., Waltham, USA
Vacuum centrifuge	Eppendorf AG, Hamburg, DE
Vortexer	Satorius AG, Göttingen, DE

Scale	Kern & Sohn GmbH, Balingen-Frommen, DE
Waterbath	Greiner Bio-One International GmbH, Kremsmünster, AT
Western blot apparatus	BioRad Laboratories, München, DE
Centrifuge	Eppendorf AG, Hamburg, DE
Sonicator	Thermo Fisher Scientific Inc., Waltham, USA

3.1.2 Chemicals

Fig. 3: Chemicals. All chemicals used in this work and their manufacturers (company name, location) are listed.

Chemical	Company
Accutase	Thermo Fisher Scientific Inc., Waltham, USA
Acetonitrile	Sigma Aldrich Chemie GmbH, Taufkirchen, DE
Ammonium bicarbonate	Sigma Aldrich Chemie GmbH, Taufkirchen, DE
1x PBS	Thermo Fisher Scientific Inc., Waltham, USA
Aqua dest	ELGA LabWater Ltd., High Wycombe, UK
BSA	Carl Roth GmbH + Co. KG, Karlsruhe, DE
carboxylate modified magnetic beads	GE Healthcare Sera-Mag™, Chicago, USA
Coomassie	Carl Roth GmbH + Co. KG, Karlsruhe, DE
DEPC water	Thermo Fisher Scientific Inc., Waltham, USA
Dithiothreitol	Carl Roth GmbH + Co. KG, Karlsruhe, DE
DMEM	Thermo Fisher Scientific Inc., Waltham, USA
EMEM	Thermo Fisher Scientific Inc., Waltham, USA
Ethanol	Carl Roth GmbH + Co. KG, Karlsruhe, DE
FBS	Thermo Fisher Scientific Inc., Waltham, USA
Glycine	Carl Roth GmbH + Co. KG, Karlsruhe, DE
HCl 37%	Carl Roth GmbH + Co. KG, Karlsruhe, DE
Hoechst	Thermo Fisher Scientific Inc., Waltham, USA
Iodoacetamide	Carl Roth GmbH + Co. KG, Karlsruhe, DE
Methanol	Carl Roth GmbH + Co. KG, Karlsruhe, DE
Paraformaldehyde	Carl Roth GmbH + Co. KG, Karlsruhe, DE
Ponceau S	Carl Roth GmbH + Co. KG, Karlsruhe, DE
Prestained protein ladder	Thermo Fisher Scientific Inc., Waltham, USA
Penicillin-Streptomycin Solution	Sigma Aldrich Chemie GmbH, Taufkirchen, DE
RPMI	Thermo Fisher Scientific Inc., Waltham, USA
SDC	Sigma Aldrich Chemie GmbH, Taufkirchen, DE

SDS	Carl Roth GmbH + Co. KG, Karlsruhe, DE
TEAB	Sigma Aldrich Chemie GmbH, Taufkirchen, DE
Tris base	Carl Roth GmbH + Co. KG, Karlsruhe, DE
Trypsin (MS Grade)	Promega Corporation, Madison, USA
Tween 20	Sigma Aldrich Chemie GmbH, Taufkirchen, DE

3.1.3 Kits

Fig. 4: Kits. All kits are used in this work and their manufacturers (company name, location) are listed.

kit	Company
Lipofectamine™ 3000 Transfection Reagent	Thermo Fisher Scientific Inc., Waltham, USA
SuperSignal West Pico PLUS Chemiluminescent Substrate	Thermo Fisher Scientific Inc., Waltham, USA
Pierce™BCA Protein Assay Kit	Thermo Fisher Scientific Inc., Waltham, USA
CellTiter-Glo® Luminescent Cell Viability Assay Kit	Promega Corporation, Madison, USA

3.1.4 Solutions

Solutions. All self-made solutions used are listed with the recipe.

Solution	Recipe
10x PBS	1,4 M NaCl; 27 mM KCl; 100 mM Na_2HPO_4; 18 mM KH_2PO_4; in Aqua dest; pH 7,4
10x Running buffer	0.25 M Tris base; 1.92 M Glycine; 20 % Methanol; in Aqua dest.
10x Sandwich buffer	250 mM Tris base; 1.92 M Glycine; 10 % Methanol; in Aqua dest.
5% Blocking buffer	5% milk powder; a little sodium azide; in TBST.
Cell Freezing Medium	90% FBS; 10% DMSO
RIPA buffer	50 mM Tris base; 150 mM NaCl; pH 8.0 (HCl); 1 % NP40, 0.5% Natriumdeoxycholat; 1 mM EDTA; je 10 ml 1 Tablet Complete Mini
Stripping buffer	100 mM Glycine; in Aqua dest; pH2,0 (HCl)
PBS-T	10 % 10x PBS; 0,1 % Tween 20; in Aqua dest
TBS-T	10 % 10x TBS; 0,1 % Tween 20; in Aqua dest
SDC buffer	0.1 M Triethylammoniumbicarbonate and 1 % Sodiumdeoxycholate

two-buffer system	buffer A: 0.1% FA in H_2O, buffer B: 0.1% FA in ACN

3.1.5 Antibodies

Fig. 5: Primary antibodies. The primary antibodies used are listed with the manufacturer (company name, location) and the corresponding dilutions.

Antibody	Dilution	Company
Anti-CCT2 antibody	1:1000	Abcam Limited, Cambridge, UK
CCT4 Polyclonal antibody	1:1000	Proteintech GmbH, Planegg-Martinsried, DE
CCT8 Polyclonal antibody	1:1000	Proteintech GmbH, Planegg-Martinsried, DE
anti-C-MYC antibody	1:1000	Zeta Corporation, Sierra Madre, CA
anti-Actin	1:1000	Merck KGaA, Darmstadt, DE

Fig. 6: Secondary antibodies. The secondary antibodies used are listed with the manufacturer (company name, location) and the corresponding dilutions.

Antibody	Dilution	Company
Anti-Rabbit IgG	1:2500	Promega Corporation, Madison, USA
Anti-mouse IgG	1:2500	Promega Corporation, Madison, USA

3.1.6 Biomaterials

Fig. 7: Cell lines. All available cell lines used are listed with information on the cell types and suppliers.

Cell line	Cell type	Subtype	Supplier
DAOY	Medulloblastoma (Human cells)	SHH	ATCC
D283Med	Medulloblastoma (Human cells)	Group 3/4	ATCC
HD-MB03	Medulloblastoma (Human cells)	Group 3	Dr. Nina Struve
D425Med	Medulloblastoma (Human cells)	Group 3	Merck

3.1.7 siRNAs

Fig. 8: All siRNAs used are listed with information on the sequences and companies.

siRNA	Sequence (5’-3’)	Company
CCT-8 siRNA	GUUGAUAAAGACUGCUGAA	Eurofins, DE
Control siRNA	UAGCGACUAAACACAUCAA	Eurofins, DE

3.1.8 Software and databases

Fig. 9: Software. All software programs and online search engines used in addition to the operating programs for the measuring devices are listed, along with the manufacturer (company name, location) and website address.

Name	Details
EndNote X9	Thomas Reuters, Philadelphia, USA
Proteome Discoverer v.3.0	Thermo Fisher Scientific, USA
GraphPad Prism	GraphPad Software Inc., Boston, USA
ImageJ	http://imagej.net
Swiss-Prot	https://www.expasy.org/sprot
NCBI	https://www.ncbi.nlm.nih.gov/
SPSS Statistics 27	IBM, Armonk, USA
Windows Office 365	Microsoft, Redmond, USA
cellSens APEX	Olympus Corporation, Tokyo, JP

3.1.9 Statistical analysis

All data were statistically analyzed using SPSS Statistics 27 software from IBM, USA. The closeness between two groups of data with small sample content and normal distribution was determined using independent sample t-test; the comparison between multiple groups was performed using one-way ANOVA. LC-MS/MS data analysis was performed using GraphPad Prism and a multiple unpaired t-test including Benjamini Hochberg p-value correction. When adj. p-value < 0.05, the difference was considered statistically significant.

3.2 Methods

3.2.1 Cell culture

3.2.1.1 Cell recovery

(1) After taking the frozen cells out of the -80℃ refrigerator, shake them continuously in a 37℃ water bath to promote their thawing.

(2) Transfer them to a 15ml falcon tube, add 10ml DMEM complete medium, blow gently, centrifuge at 1000rpm, 5min, and discard the supernatant.

(3) Add 10ml DMEM complete medium, blow gently, inoculate in a 10cm culture flask, and culture in a cell incubator at 37℃ and 5% CO_2.

3.2.1.2 Cell passaging

3.2.1.2.1 Passage adherent cells

(1) When the cell density reaches 80% to 90%, use a pipette to remove the culture medium and wash twice with 10ml PBS.
(2) Add 3ml accutase to the flask and gently shake the culture flask to allow the digestion solution to flow over all cell surfaces. Return the culture flask to the incubator and take it out after 5 min.
(3) Directly add the same volume of complete culture medium to terminate digestion.
(4) Use a pipette to absorb the culture medium in the flask and repeatedly blow the cells on the bottom.
(5) Transfer the cell suspension to a 15ml falcon tube and centrifuge at 1000rmp for 5min.
(6) Remove the culture medium and add new culture medium, and repeatedly blow to make the cells detach from the bottom to form a cell suspension.
(7) Inoculate at 1×10^6/flask and continue to culture in a cell culture incubator containing 5% CO_2.

3.2.1.2.2 Passage suspension cells

(1) Transfer the cells and culture medium into a 15 ml centrifuge tube.
(2) Centrifuge at 700 rpm for 3 min.
(3) Discard the supernatant and add new culture medium to the falcon tube, and pipette to form a cell suspension.
(4) Inoculate at 1×10^6/flask and continue to culture in a cell culture incubator containing 5% CO_2.

3.2.1.3 Cell freezing

(1) When the cell density reaches 80%-90%, remove the culture medium with a pipette and wash twice with 10ml PBS.

(2) Add 3ml accutase to the flask and gently shake the culture flask to allow the digestion solution to flow over all cell surfaces. Return the culture flask to the incubator and take it out after 5 min.

(3) Directly add the same volume of complete culture medium to terminate digestion.

(4) Use a pipette to absorb the culture medium in the flask and repeatedly blow the cells on the bottom.

(5) Transfer the cell suspension to a 15ml falcon tube and centrifuge at 1000rmp for 5min.

(6) Remove the culture medium.

(7) Add 1 ml of freezing solution (90% culture medium, 10% DMSO) and repeatedly blow the cells on the bottom. Transfer all liquid to a cryotube.

(8) Directly place the cryotube into the cell freezing box and then into the -80ºC low-temperature freezer overnight, then place in liquid nitrogen for long-term storage.

3.2.1.4 Cell culture conditions

All cell culture flasks and plates are placed in the incubator at 37℃ and 5% CO_2.

The specific cell culture conditions are shown below.

Cell line	**Culture condition**	**Culture medium**
DAOY	adherent	DMEM, 10% FBS, 1%P/S
D283Med	adherent	EMEM, 10%FBS, 1%P/S
HD-MB03	adherent	RPMI, 10% FBS, 1%P/S
D425Med	suspension	DMEM, 10% FBS, 1%P/S

3.2.2 Transfection

3.2.2.1 DAOY cell line

(1) Seed DAOY cells to be 70% confluent at transfection in 6-well plate.

(2) Let cells grow for 24 hours

(3) Dilute 3.75ul Lipofectamine™ 3000 Reagent in 125ul Opti-MEM™ Medium (2 tubes)– Mix well.

(4) Prepare master mix of siRNA by diluting 2ul siRNA in 125ul Opti-MEM™ Medium – Mix well.

(5) Add Diluted siRNA to each tube of Diluted Lipofectamine™ 3000 Reagent (1:1 ratio).

(6) Incubate 15 min at RT.

(7) Add 250ul siRNA-lipid complex to cells.

(8) Culture in a cell incubator at 37℃ and 5% CO_2.

(9) 3 days later, analyze transfected cells.

3.2.2.2 D283Med cell line

(1) Seed D283 cells to be 50% confluent at transfection in 6 well plate.

(2) Let cells grow for 24 hours

(3) Dilute 3.75ul Lipofectamine™ 3000 Reagent in 125ul Opti-MEM™ Medium (2 tubes).

(4) Prepare master mix of siRNA by diluting 2ul siRNA in 125ul Opti-MEM™ Medium.

(5) Add Diluted siRNA to each tube of Diluted Lipofectamine™ 3000 Reagent (1:1 ratio).

(6) Incubate 15 min at RT.

(7) Add 250ul siRNA-lipid complex to cells.

(8) Culture in a cell incubator at 37℃ and 5% CO_2.

(9) 24 hours later, repeat step 2-7.

(10) 3 days later, analyze transfected cells.

3.2.2.3 HD-MB03 cell line

(1) Seed HD-MB03 cells to be 50% confluent at transfection in 6-well plate.

(2) Let cells grow for 24 hours

(3) Dilute 7.5ul Lipofectamine™ 3000 Reagent in 125ul Opti-MEM™ Medium (2 tubes).

(4) Prepare master mix of siRNA by diluting 4ul siRNA in 125ul Opti-MEM™ Medium.

(5) Add Diluted siRNA to each tube of Diluted Lipofectamine™ 3000 Reagent (1:1 ratio).

(6) Incubate 15 min at RT.

(7) Add 250ul siRNA-lipid complex to cells.

(8) Culture in a cell incubator at 37℃ and 5% CO_2.

(9) 24 hours later, repeat step 2-7.

(10) 3 days later, analyze transfected cells.

3.2.2.4 D425Med cell line

(1) Seed 1 x 10^6 D425 cells at transfection in 6 well plate.

(2) Dilute 3.75ul Lipofectamine™ 3000 Reagent in 125ul Opti-MEM™ Medium (2 tubes).

(3) Prepare master mix of siRNA by diluting 2ul siRNA in 125ul Opti-MEM™ Medium.

(4) Add Diluted siRNA to each tube of Diluted Lipofectamine™ 3000 Reagent (1:1 ratio).

(5) Incubate 15 min at RT.

(6) Add 250ul siRNA-lipid complex to cells.

(7) Culture in a cell incubator at 37℃ and 5% CO_2.

(8) 24 hours later, repeat step 2-7.

(9) 3 days later, analyze transfected cells.

3.2.3 Western blot

3.2.3.1 Extract protein

(1) Remove the culture medium with a pipette and wash twice with 10ml PBS.

(2) After centrifugation, remove the culture medium and add 100 µl of RIPA buffer.

(3) Transfer tumor cells to a 1.5 ml eppendorf tube.

(4) The resulting suspension was then mixed and homogenized on a vortexer.

(5) During the 30 min incubation on ice, the samples were vortexed regularly every 10 min.

(6) Subsequently, the samples were centrifuged at 12,000 rpm and 4 °C for 10 min.

(7) The supernatant containing the solubilized cell proteins produced in this step was transferred to a new 1.5 ml centrifuge tube using a pipette.

(8) The obtained samples were then stored at -80°C until the protein concentration was determined or further used.

3.2.3.2 Measure protein concentration

(1) Prepare a 96 well plate and make a duplicate for each sample.

(2) Dilute the standard which is a bovine serum albumin with 2mg/ml stock solution.

(3) Start with pipetting ddH_2O: 5µl ddH_2O + 5µl of diluted standard, 9µl ddH_2O + 1µl of sample, 10µl ddH_2O in blank wells.

(4) Add 200µl Bradford Buffer in each well.

(5) Choose the right assay and check the standard curve.

(6) Calibrate concentration. and get a table of the protein concentration.

(7) Add 1/4 of the volume of Loading Buffer 4x (with Laemmli). Add sample 10 to 50µg.

(8) Put it on 98°C for 5min.

(9) Put it shortly on ice, spin it down and then store it at -20°C until the next step. Or store it at -80°C for long time (avoid freeze/ thaw).

3.2.3.3 Sodium dodecyl sulfate polyacrylamide gel electrophoresis (SDS-PAGE)

We use precast gradient Gel (Bio-Rad Laboratories GmbH, Feldkirchen, DE).

(1) Remove the stripe on the gel and comb.

(2) Place the gel in the electrophoresis box.

(3) Fill the middle full with the buffer and on the side minimum to the level where the stripe was.

(4) Wash each well with the Running Buffer.

(5) Then load 5µl of the protein Marker Ladder (M).18µl of the sample. 6µl Loading Buffer (1x) if necessary (L).

(6) Close the lid.

(7) When you start the electrophoresis, leave it the first 5 min outside on 150V, then put the box carefully on ice for 30-60min at 200V.

(8) Stop the gel-electrophoresis when the loading buffer reaches the bottom of the gel.

(9) Open the gel and cut the unnecessary parts.

(10) Wash the gel in the Western Transfer Buffer.

3.2.3.4 Protein electrophoresis

When transfer the proteins from the gel to the membrane, don’t touch the membrane with the fingers.

(1) Make sure when you arrange the “sandwich” that everything is wet and covered with the sandwich buffer and that there are no bubbles on the membrane.

(2) The gel should be closer to the ANODE side (black) and the membrane to the KATODE side (see-through).
(3) When you put the “sandwich” into the electrophorese box, make sure the black side of the plastic sandwich holder faces the black side of the box.
(4) Fill the box up with the Western Transfer Buffer, covering the gel and the membrane.
Put the box on ice and run for 60min on 100V.

3.2.3.5 Block protein

(1) Open the “sandwich” and trim the membrane that is not necessary.
(2) Put Blocking Buffer in a box, then the membrane.
(3) Put the box on a rocker for 60min.
(4) Remove blocking Buffer.

3.2.3.6 Detect target protein

3.2.3.6.1 1stAB

(1) Take 15ml falcons: 5ml of Blocking Buffer (TBS + Tween (TBST) + 5% milk + knife point Sodium Azide) + 1stAB (1:1000)
(2) Put into the box and with the membrane and leave overnight on shaker in 4°C.
(3) Wash the membrane for 3 times for five min with TBST.

3.2.3.6.2 2nd antibody

(1) Take 15ml falcons: 5ml of Blocking Buffer (TBS + Tween (TBST) + 5% milk + knife point Sodium Azide) + 2ndAB (1:2500)
(2) Shake 60min at RT on the shaker.
(3) Wash the membrane for 3 times for five min with TBST.

3.2.3.6.3 Visualize binding

(1) Pico reagent a and b. Mix it 1:1 (1ml per blot in total).
(2) Put in plastic box 1ml of the Pico mixture and incubate with face down for 5min.
(3) Put the membrane on see-through foil and then visualize with BioRad ChemiDoc MP imaging system.

(4) Normalize the detected protein of interest to the total amount of protein and quantify. Housekeeping proteins for control should be detected on the same membrane.

3.2.4 Cell proliferation assay

(1) Prepare a 96 well white plate and make a four compound holes for each sample.

(2) Seed 1 x 10^4 transfected cells/ well in 100 µl culture medium and culture in a cell incubator at 37℃ and 5% CO_2 for 2 days.

(3) Leave the 96 well white plate at RT for 30 min.

(4) Thaw CellTiter-Glo® Buffer and CellTiter-Glo® Substrate and equilibrate to RT.

(5) Transfer the entire bottle of CellTiter-Glo® Buffer to the brown bottle containing CellTiter-Glo® Substrate.

(6) Shake the contents for 1 min to obtain a homogenous CellTiter-Glo® Reagent.

(7) Directly add an equal volume of CellTiter-Glo® Reagent to each well of culture medium.

(8) Mix for 2 min on an orbital shaker to induce cell lysis.

(9) Incubate the plate at RT for 10 min to allow the luminescent signal to stabilize.

(10) Record the luminescent signal by GloMax® Discover System.

3.2.5 Vincristine treatment

(1) Prepare a 96 well white plate and make a four compound holes for each sample.

(2) Seed 1 x 10^4 transfected cells/ well in 100 µl culture medium and culture in a cell incubator at 37℃ and 5% CO_2 for 24 hours.

(3) Remove culture medium and add 100 µl/well fresh culture medium with vincristine (1ng/ml, 5ng/ml, 10ng/ml, 50ng/ml, 100ng/ml, 1µg/ml).

(4) Culture in a cell incubator at 37℃ and 5% CO_2 for 2 days.

(5) Leave the 96 well white plate at RT for 30 min.

(6) Thaw CellTiter-Glo® Buffer and CellTiter-Glo® Substrate and equilibrate to RT.

(7) Transfer the entire bottle of CellTiter-Glo® Buffer to the brown bottle containing CellTiter-Glo® Substrate.

(8) Shake the contents for 1 min to obtain a homogenous CellTiter-Glo® Reagent.

(9) Directly add an equal volume of CellTiter-Glo® Reagent to each well of culture medium.

(10) Mix for 2 min on an orbital shaker to induce cell lysis.

(11) Incubate the plate at RT for 10 min to allow the luminescent signal to stabilize.

(12) Record the luminescent signal by GloMax® Discover System.

3.2.6 Cell migration assay

(1) 2 ml of cell culture medium containing 10% FCS was pipetted into each well of a 6-well plate.

(2) Insert the transwell insert into the well using sterile forceps.

(3) Resuspend the cells in serum-free medium and seed onto the transwell polycarbonate membrane at $1x10^6$ cells/ml and incubate at 37°C for 24 hours.

(4) Fix the cells on both sides of the membrane with 4% PFA for 15 minutes at RT.

(5) Discard all 4% PFA and wash each well twice with 1xDPBS.

(6) Visualize the nuclei using fluorescent labeling by incubating 2 ml Hoechst (10 µg/ml) in 1xDPBS on the polycarbonate membrane for 15 minutes in the dark.

(7) After washing twice more with 1xDPBS, generate fluorescent images of Hoechst staining of the entire well using Olympus APX100 microscope and cellSens APEX software to get an overview of all cells.

(8) Non-migrated cells on the upper chamber membrane were removed with a cotton swab.

(9) New fluorescent images show cells that migrated underneath the membrane.

3.2.7 Proteomics analyses via mass spectrometry (This work was done by the core facility proteomics at the UKE.)

3.2.7.1 Optimized processing of proteins

(1) Proteins were sonicated for 5 pulses at 30 Hz.

(2) Protein pellets were resuspended in 200 µL SDC buffer and heated at 95 °C for 5 minutes.

(3) Samples were diluted to 20 µg of protein in 50 µL buffer.

(4) Samples were heated in 10 mM dithiothreitol for 30 min at 56 °C.

(5) Samples were heated in 20 mM iodoacetamide for 30 min at 37 °C in the dark.

(6) Samples were dissolved to a concentration of 70% acetonitrile.

(7) 1 µL carboxylate modified magnetic beads at 1:1 (hydrophilic/ hydrophobic) in methanol were added.

(8) Samples were shaken at 1400 rpm for 18 min at room temperature.

(9) Tubes were placed on a magnetic rack and the supernatant was removed.
(10) Magnetic beads were washed two times with 100% CAN.
(11) Magnetic beads were washed two times with 70% Ethanol on the magnetic rack.
(12) Samples were resuspended in 50 mM ammonium bicarbonate.
(13) Samples were digested with trypsin at 1:100 (enzyme: protein) ratio at 37 °C overnight while shaking at 1400 rpm.
(14) Tryptic peptides were bound to the beads by adding 95% ACN and shaken at 1400 rpm for 10 min at room temperature.
(15) Tubes were placed on the magnetic rack, the supernatant was removed, and the beads were washed two times with 100% ACN.
(16) Elution was performed with 2% DMSO in 1% formic acid.
(17) The supernatant was dried in a vacuum centrifuge and stored at -20°C until further use.

3.2.7.2 Liquid chromatography-mass spectroscopy

(1) Chromatographic separation of peptides was achieved with a two-buffer system on a nano-UHPLC.
(2) Attached to the UHPLC was a peptide trap (100 µm x 20 mm, 100 Å pore size, 5 µm particle size, C18, Nano Viper, Thermo Fisher) for online desalting and purification, followed by a 25 cm C18 reversed-phase column (75 µm x 250 mm, 130 Å pore size, 1.7 µm particle size, peptide BEH C18, nanoEase, Waters).
(3) Peptides were separated using an 80 min method with linearly increasing ACN concentration from 2% to 30% ACN over 60 minutes.
(4) Eluting peptides were ionized using a nano-electrospray ionization source (nano-ESI) with a spray voltage of 1,800 V and analyzed in data dependent acquisition (DDA) mode.
(5) For each MS1 scan, ions were accumulated for a maximum of 120 milliseconds or until a charge density of 2 x 10^5 ions (AGC Target) was reached.
(6) Fourier-transformation based mass analysis of the data from the orbitrap mass analyzer was performed covering a mass range of m/z 400 – 1,300 with a resolution of 120,000 at m/z = 200.
(7) Peptides with charge states between 2+ - 5+ above an intensity threshold of 1,000 were isolated within a m/z 1.6 isolation window in Top Speed mode for 3 seconds from each

precursor scan and fragmented with a normalized collision energy of 30% using higher energy collisional dissociation (HCD).
(8) MS2 scanning was performed, using an ion trap mass analyzer at a rapid scan rate, covering a mass range starting at m/z 120 and accumulated for 60 ms or to an AGC target of 1×10^5.
(9) Already fragmented peptides were excluded for 30 s.

3.2.7.3 LC-MS/MS data analysis

LC-MS/MS data were searched with the Sequest algorithm integrated into the Proteome Discoverer software (v.3.0, Thermo Fisher Scientific) against a reviewed human Swiss-Prot database, obtained in April 2021, containing 20,365 entries. Carbamidomethylation was set as a fixed modification for cysteine residues. The oxidation of methionine at the peptide N-terminus, as well as acetylation of the protein N-terminus were allowed as variable modifications. A maximum number of two missing tryptic cleavages was set. Peptides between 6 and 144 amino acids were considered. A strict cutoff (FDR < 0.01) was set for peptide and protein identification. Quantification was performed using the Minora Algorithm, implemented in Proteome Discoverer. Obtained protein abundances were log2-transformed and normalized by column-median normalization.

4. Results

4.1 siRNA transfection and western blot experiments confirmed the reduction of CCT-8 expression

In order to analyze the functional role of the CCT complex in medulloblastoma, we aimed to downregulate the CCT complex via knockdown of CCT-8. We therefore transfected medulloblastoma cell lines with a siRNA targeting CCT-8. A non -target siRNA was used as control. Through western blot experiments, we confirmed that the expression of the CCT-8 protein in transfected medulloblastoma cell lines was significantly reduced (Figure 1, Supplementary Figure 1-4). A paired t-test was used for statistical analysis comparing the different conditions. Relative quantitative analysis showed that in the four medulloblastoma cell lines analyzed, the expression of the CCT-8 protein was significantly reduced in cells transfected with target CCT-8 siRNA (CCT-8 knockdown) compared to untreated cells, and cells transfected with non-target siRNA (control cell). There was no significant difference in the expression of CCT-8 protein between untreated cells and control cells (Figure 2, Supplementary Table 1-4).

4.2 Effects of reduced CCT-8 expression on the expression of other proteins

In order to analyze the effect of CTT-8 downregulation on other CCT components we performed further western blot experiments displaying the expression of CCT-2 and CCT-4 in CCT-8 knockdown cells, untreated cells, and control cells (Figure 3-6, Supplementary Figure 5-8, Supplementary Table 1-4). Additionally, as high CCT component abundance was found in MYC activated Group3 medulloblastoma, we analyzed C-MYC expression in medulloblastoma cells after CCT-8 knockdown (Figure 3-6, Supplementary Figure 5-8, Supplementary Table 1-4). A paired t-test was used for statistical analysis. Relative quantitative analysis showed that in the four medulloblastoma cell lines, there was no significant change in the expression of CCT-2 and CCT-4 proteins after CCT-8 knockdown (Figure 3-6, Supplementary Figure 5-8, Supplementary Table 1-4). In DAOY and D283 cell lines, C-MYC protein expression was significantly reduced after CCT-8 knockdown (Figure 3-4, Supplementary Figure 5-6, Supplementary Table 1-2). In the HD-MB03 cell line, there was no significant change in C-MYC protein expression after CCT-8 knockdown (Figure 5, Supplementary Figure 7, Supplementary Table 3). In the D425 cell line, C-MYC protein expression was significantly increased after CCT-8 knockdown (Figure 6, Supplementary Figure 8, Supplementary Table 4).

4.3 Effect of reduced CCT-8 expression on the proliferative behavior of medulloblastoma

To analyze the proliferation capacity of medulloblastoma cell lines after CCT-8 knockdown, the CellTiter Glo assay was performed. One-way ANOVA was used for statistical analysis. Quantitative analysis showed that in the four medulloblastoma cell lines, the proliferation capacity of cells was significantly decreased after CCT-8 knockdown (Figure 7, Supplementary Table 5-8).

4.4 Effect of reduced CCT-8 expression on the migration behavior of medulloblastoma cells

Cell migration, spreading and metastases are a hallmark of cancer. In order to analyze the migration ability of medulloblastoma cells after CCT-8 knockdown, the transwell assay was performed. As this assay is only suited for adherent cells, the D425 cell line, which grows in suspension could not be analyzed. A paired t-test was used for statistical analysis. Relative quantitative analysis showed that in the four medulloblastoma cell lines, the migration ability of cells was significantly reduced after CCT-8 knockdown (Figure 8, Supplementary Table 9-11).

4.5 Effect of reduced CCT-8 expression on drug resistance in medulloblastoma

Previous proteome studies on medulloblastoma showed that the CCT components are reduced in WNT medulloblastoma and highly expressed in Group 3 medulloblastoma (Godbole et al., 2024). WNT medulloblastomas respond well to chemotherapy and have been described as tumors with relatively good prognosis, whereas Group 3 medulloblastoma are aggressive and respond poorly to therapy. We therefore hypothesized that the CCT complex might impact on the effectiveness of chemotherapy. We focused on vincristine, which is commonly applied to medulloblastoma patients in clinics (Prados, 2023). To analyze the drug sensitivity of medulloblastoma cell lines after CCT-8 knockdown, the CellTiter Glo assay was performed, and results were compared to untreated and control cells (non-target siRNA). Quantitative analysis showed that in all four medulloblastoma cell lines, a knockdown of CCT-8 resulted in a (at least slightly) increased sensitivity of cells towards vincristine treatment, depicted by a shift of the IC50 values to lower values (Figure 9, Supplementary Table 12-23).

4.6 Proteomic analysis after CCT-8 knockdown in medulloblastoma

In order to confirm and extend the results of Western Blot analyses, mass spectrometry based proteome analyses of medulloblastoma cells was performed and revealed that expression of multiple CCT subunits was affected by CCT-8 knockdown (Figure 10). Expression of the CCT-2 subunit was downregulated following knockdown of CCT-8 protein in DAOY and D425 cell lines. Expression of the CCT-6A and CCT-7 subunits was downregulated following knockdown of CCT-8 protein in the DAOY cell line. Expression of CCT-3, CCT-4 and CCT-5 subunits was significantly downregulated following the knockdown of CCT-8 protein in all four cell lines. In contrast, the expression of C-MYC associated proteins was not affected by CCT-8 knockdown (Figure 11). These data were generated by the Proteome Facility at UKE and were analyzed with kind help of Ms. Antonia Gocke.

5. Discussion

Brain tumors are very common among childhood malignant tumors, accounting for about 20% of all childhood malignant tumors, and their incidence rate is second only to leukemia (Subramanian et al., 2023). The location of brain tumors is related to age. Childhood brain tumors are more common in the infratentorial, posterior cranial fossa and midline areas (Lutz et al., 2022). Common brain tumors in children include medulloblastoma, astrocytoma, craniopharyngioma, ependymoma, brain stem glioma, etc. (Ozair et al., 2022). The most commonly used treatment for intracranial tumors is surgical resection (Krist et al., 2022), but in order to avoid the removal of normal brain tissue and the characteristics of malignant tumors with extensive invasive growth, it is very difficult to completely remove tumor tissue surgically. Therefore, it is crucial to develop more accurate diagnostic methods and explore more effective tumor treatment methods.

Medulloblastoma is the most common malignant nervous system tumor in children. Its occurrence is related to the activation of multiple oncogenes and related signaling pathways (Cooney et al., 2023). Researchers have found that medulloblastoma can be divided into multiple different subtypes (Wang et al., 2022； Godbole et al., 2024). These subtypes have significant differences in gene expression, gene mutations and DNA methylation. Further studies have shown that these subtypes are closely related to the prognosis and treatment response of medulloblastoma patients. Previous studies used samples from medulloblastoma patients to conduct multi-omic analyses, integrating DNA methylomics, transcriptomics and proteomics, and found that there were differences in the expression and protein abundances of multiple genes in medulloblastoma samples of different molecular subtypes (Godbole et al., 2024). Components of the CCT complex were revealed to be specifically differentially abundant based on proteins, whereas RNA expression was relatively similar. As the CCT complex was revealed as a novel proteome characteristic in medulloblastoma subtypes, being specifically low expressed in relatively benign WNT medulloblastoma and high expressed in aggressive Group 3 medulloblastoma, we hypothesized that CCT component abundance might be related to tumor growth, aggressiveness and even therapy response. Therefore, we performed multiple functional analyses studying behavior of medulloblastoma cells after CCT-8 knockdown, including the analyses of tumor proliferation and migration behavior, drug sensitivity, as well as proteomic analyses.

Chaperone, also known as molecular chaperone. It is a protein complex with a size of about 1MDa. It consists of 7-9 subunits and forms a double ring structure. There is a protein folding chamber in the center of each ring (Nishimura et al., 2020). Human health depends on correctly folded and functioning proteins as protein misfolding may induce a variety of diseases, such as cancer, neurodegenerative diseases, etc. (Bhattacharya et al., 2024; Rinauro et al., 2024). The CCT family is a member of the molecular chaperone, which can help other proteins to assemble and fold correctly and assist in the degradation of misfolded proteins (Que et al., 2024). The CCT family is a class of evolutionarily conserved complexes that are involved in the folding of about 10% of the proteome in cells (Smith et al., 2022). Previous studies have found that CCT family genes are closely related to the occurrence and development of tumors (Lv et al., 2022).

Cell proliferation, migration and invasion are the main driving factors for tumor occurrence and progression (Novikov et al., 2021), and these processes are accompanied by the interaction of molecular chaperone CCT with its substrates such as actin, tubulin, VHL, STAT3 and other proteins (Svanström et al., 2016). Studies have shown that CCT can not only function as a complex, but also play a role in cell proliferation and migration as a monomer (Zeng et al., 2024). Therefore, the activity of CCT and its subunits may affect the occurrence and development of cancer. Among them, CCT-8 is highly correlated with the occurrence, development and prognosis of several malignant tumors such as glioma and breast cancer (Liao et al., 2021; Wang et al., 2021). However, the role of CCT-8 in medulloblastoma remains unknown. Therefore, in this study, four medulloblastoma cell lines with low expression of CCT-8 were constructed to explore the function of CCT-8 in medulloblastoma. Meanwhile, proteomic was used to analyze the expression of different CCT subunits in medulloblastoma cell lines of different molecular subtypes when CCT-8 was downregulated. Proteomic results showed that in different subtypes of medulloblastoma, CCT family members can interact with each other and act as monomers, which is consistent with previous studies on other tumor entities (Zeng et al., 2024).

The MYC protein family plays an important role in the maturation and differentiation of embryonic neural stem cells and the development of the central nervous system. MYC protein

affects cell proliferation, differentiation and apoptosis by regulating the expression of multiple genes (Zaytseva et al., 2020). Overexpression of C-MYC can promote the rapid proliferation of medulloblastoma cells, inhibit cell differentiation, and increase the survival rate of tumor cells (Roussel et al., 2013). Similarly, studies on the regulatory effects of CCT subunits on tumor cells showed effects on cell proliferation, invasion, migration, apoptosis, and drug resistance (Zheng et al., 2023). As the CCT complex was found to be highly abundant in C-MYC activated Group 3 medulloblastoma (Godbole et al. 2024) we hypothesized that there might be a functional link between CCT and C-MYC. Therefore, we downregulated the expression of CCT-8 protein in medulloblastoma cell lines and explored the expression of C-MYC protein and C-MYC associated proteins. We found that compared with wild-type medulloblastoma cell lines and control medulloblastoma cell lines, the expression level of C-MYC protein was also affected along with the downregulation of CCT-8. However, C-MYC associated proteins were not significantly altered. The potential cross-regulatory mechanism between the two therefore needs further study.

In the chemotherapy of medulloblastoma, many chemotherapeutic drugs inhibit tumor cell growth by interfering with the mitotic process of cancer cells. Such drugs include the vinca alkaloids, vincristine, vinblastine, vinorelbine, vindesine, and vinflunine (Banyal et al., 2023). We applied vincristine to medulloblastoma cells and this study investigated the relationship between the molecular subtypes of medulloblastoma and related clinical therapeutic drugs. We found that vincristine had detected a different inhibitory effect on different medulloblastoma cell lines that potentially represent different molecular subtypes (see also methods). Compared with wild-type medulloblastoma cell lines and control cell lines, knockdown of CCT-8 expression in medulloblastoma cell lines enhanced the sensitivity of cells to vincristine treatment. These findings provide a basis for future developments of personalized treatment of medulloblastoma subtypes.

In summary, this study preliminarily confirmed that the expression level of CCT-8 is positively correlated with the malignant biological behavior of medulloblastoma, and downregulation of CCT-8 can reduce the proliferation, invasion and metastasis of medulloblastoma. This shows that CCT-8 may be closely related to the occurrence and development of medulloblastoma, and can be used as a potential tumor marker and an indicator for judging the survival

prognosis of tumor patients. However, the cancer-promoting mechanism of CCT-8 in medulloblastoma is still unclear. CCT-8 may be related to C-MYC and may be related to the prognosis of medulloblastoma. However, in medulloblastoma, the gene and protein interaction network and biological pathways related to CCT-8 still need more detailed analysis.

In future studies, the specific molecular mechanism of CCT-8 in promoting medulloblastoma growth and therapy resistance should be analyzed. In addition, further clinical trials are needed to verify its potential of CCT components as molecular markers for poor prognosis.

6. Summary

In this study we performed multiple functional experimental methods to examine the effects of low expression of CCT-8 in four human medulloblastoma cell lines, namely DAOY, D283Med, HD-MB03, and D425Med. This was tested by a knockdown via transfection with a siRNA targeting CCT-8 and an unspecific siRNA control. We characterized the CCT-8 knockdown and its effects through the expression analysis of multiple CCT-8 related proteins via Western Blotting and mass spectrometry, the proliferation ability through a CellTiter Glo Assay, cell migration using a migration assay, and finally cell survival ability in different concentrations of the cytostatic vincristine.

We could show a significant knockdown of CCT-8 after siRNA transfection. Other components of the CCT complex were not significantly reduced in Western Blot experiments but showed a reduction in quantitative protein analyses using mass spectrometry. Following CCT-8 knockdown, C-MYC was lower expressed in DAOY and D283 cells, while there was an increase in expression in D425 cells. C-MYC associated proteins detected via mass spectrometry were not statistically differentially regulated in CCT-8 knockdown cells. Importantly, after CCT-8 knockdown, all tested medulloblastoma cell lines showed a reduced proliferation ability, a reduced migration behavior and a slightly increased sensitivity to vincristine.

The results of this study indicate that the high expression of CCT-8 and other components of the CCT complex may be an important factor in the malignancy of medulloblastoma. Further studies to unravel the functional relationship of CCT components and a potentially corresponding drug resistance are needed and harbor the potential for development of novel personalized therapies.

Zusammenfassung

In dieser Arbeit wurden verschiedene experimentelle Methoden angewendet, um die funktionellen Auswirkungen einer geringen CCT-8 Expression in folgenden menschlichen Medulloblastomzelllinien zu untersuchen: DAOY, D283, HD-MB03 und D425. Dies wurde durch einen Knockdown von CCT-8 mittels Transfektion mit CCT-8 spezifischer siRNA und einer unspezifischen siRNA-Kontrolle getestet. Methodisch wurde der CCT-8 Knockdown und seine funktionelle Bedeutung durch die Expressionsanalyse mehrerer CCT-8-verwandter Proteine durch Western Blotting und Massenspektrometrie, die Proliferationsfähigkeit durch einen CellTiterGlo-Test, das Migrationsverhalten mithilfe eines Migrationstests und die Überlebensfähigkeit der Zellen mit verschiedenen Konzentrationen des Zytostatikums Vincristin charakterisiert.

Wir konnten den CCT-8-Knockdown in allen Zelllinien verifizieren. Während die Expression anderer CCT Komponenten im Western Blot keinen signifkanten Unterschied zeigte, konnte die quantitative Proteinanalyse mittels Massenspektrometrie eine Herunterregulierung weiterer CTT Komponenten zeigen. C-MYC wurde in DAOY- und D283-Zellen nach CCT-8 knockdown weniger exprimiert, während es in D425-Zellen zu einer erhöhten Expression kam. In der massenspetrometrischen Messung konnte keine signifikante Veränderung von C-MYC assoziierten Proteinen festgestellt werden. Alle getesteten Medulloblastomzelllinien zeigten nach CCT-8-Knockdown eine verringerte Proliferation, ein verringertes Migrationsverhalten sowie ein leicht verbessertes Ansprechen auf die Behanldung mit Vincristin.

Die Ergebnisse dieser Arbeit zeigen, dass die hohe Expression von CCT-8 ein wichtiger Faktor in der Malignität von Medulloblastomen darstellen kann. Die Beziehung zwischen der hohen CCT-8-Expression und der damit eihergehenden Arzneimittelresistenz sollte in zukünftigen Projekten weiter untersucht werden und birgt ein Potential für neuartige personalisierte Therapieansätze bei Medulloblastomen.

7. Bibliography

Bailey, P., & Cushing, H. (1926). A classification of the tumors of the glioma group on a histogenetic basis with a correlated study of prognosis.

Schüller, U., Heine, V. M., Mao, J., Kho, A. T., Dillon, A. K., Han, Y. G., Huillard, E., Sun, T., Ligon, A. H., Qian, Y., Ma, Q., Alvarez-Buylla, A., McMahon, A. P., Rowitch, D. H., & Ligon, K. L. (2008). Acquisition of granule neuron precursor identity is a critical determinant of progenitor cell competence to form Shh-induced medulloblastoma. Cancer cell, 14(2), 123–134. doi.org/10.1016/j.ccr.2008.07.005.

Gibson, P., Tong, Y., Robinson, G., Thompson, M. C., Currle, D. S., Eden, C., Kranenburg, T. A., Hogg, T., Poppleton, H., Martin, J., Finkelstein, D., Pounds, S., Weiss, A., Patay, Z., Scoggins, M., Ogg, R., Pei, Y., Yang, Z. J., Brun, S., Lee, Y., … Gilbertson, R. J. (2010). Subtypes of medulloblastoma have distinct developmental origins. Nature, 468(7327), 1095–1099. doi.org/10.1038/nature09587.

Smith, K. S., Bihannic, L., Gudenas, B. L., Haldipur, P., Tao, R., Gao, Q., Li, Y., Aldinger, K. A., Iskusnykh, I. Y., Chizhikov, V. V., Scoggins, M., Zhang, S., Edwards, A., Deng, M., Glass, I. A., Overman, L. M., Millman, J., Sjoboen, A. H., Hadley, J., Golser, J., … Northcott, P. A. (2022). Unified rhombic lip origins of group 3 and group 4 medulloblastoma. Nature, 609(7929), 1012–1020. doi.org/10.1038/s41586-022-05208-9.Marino S. (2005). Medulloblastoma: developmental mechanisms out of control. *Trends in molecular medicine*, *11*(1), 17–22. doi.org/10.1016/j.molmed.2004.11.008.

Carta, R., Del Baldo, G., Miele, E., Po, A., Besharat, Z. M., Nazio, F., Colafati, G. S., Piccirilli, E., Agolini, E., Rinelli, M., Lodi, M., Cacchione, A., Carai, A., Boccuto, L., Ferretti, E., Locatelli, F., & Mastronuzzi, A. (2020). Cancer Predisposition Syndromes and Medulloblastoma in the Molecular Era. *Frontiers in oncology*, *10*, 566822. doi.org/10.3389/fonc.2020.566822.

Fang, F. Y., Rosenblum, J. S., Ho, W. S., & Heiss, J. D. (2022). New Developments in the Pathogenesis, Therapeutic Targeting, and Treatment of Pediatric Medulloblastoma. *Cancers*, *14*(9), 2285. doi.org/10.3390/cancers14092285.

Ellison D. (2002). Classifying the medulloblastoma: insights from morphology and molecular genetics. *Neuropathology and applied neurobiology*, *28*(4), 257–282. doi.org/10.1046/j.1365-2990.2002.00419.x.

Raffel C. (2004). Medulloblastoma: molecular genetics and animal models. *Neoplasia (New*

York, N.Y.), *6*(4), 310–322. doi.org/10.1593/neo.03454.

Ryzhova, M. V., Zheludkova, O. G., Kumirova, É. V., Shishkina, L. V., Panina, T. N., Gorelyshev, S. K., Khukhlaeva, E. A., Mazerkina, N. A., Matuev, K. B., Medvedeva, O. A., Tarasova, E. M., Kholodov, B. V., & Kapitul'skaia, O. I.u (2013). Characteristics of medulloblastoma in children under age of three years. *Zhurnal voprosy neirokhirurgii imeni N. N. Burdenko*, *77*(1), 3–11.

Meister, M., Lin, J. J., Bach, S. E., Kapileshwarkar, Y., & Kumar, P. (2022). Medulloblastoma Presenting As Isolated Leptomeningeal Enhancement With No Primary Mass. *Cureus*, *14*(7), e26598. doi.org/10.7759/cureus.26598.

Varan, A., Sari, N., Akalan, N., Söylemezoğlu, F., Akyüz, C., Kutluk, T., & Büyükpamukçu, M. (2006). Extraneural metastasis in intracranial tumors in children: the experience of a single center. *Journal of neuro-oncology*, *79*(2), 187–190. doi.org/10.1007/s11060-006-9123-3.

Rickert C. H. (2003). Extraneural metastases of paediatric brain tumours. *Acta neuropathologica*, *105*(4), 309–327. doi.org/10.1007/s00401-002-0666-x.

Campbell, A. N., Chan, H. S., Becker, L. E., Daneman, A., Park, T. S., & Hoffman, H. J. (1984). Extracranial metastases in childhood primary intracranial tumors. A report of 21 cases and review of the literature. *Cancer*, *53*(4),974–981.doi.org/10.1002/1097-0142(19840215)53:4<974::aid cncr2820530426>3.0.co;2-c.

Mazloom, A., Zangeneh, A. H., & Paulino, A. C. (2010). Prognostic factors after extraneural metastasis of medulloblastoma. *International journal of radiation oncology, biology, physics*, *78*(1), 72–78. doi.org/10.1016/j.ijrobp.2009.07.1729.

Merchant, T. E., Kun, L. E., Krasin, M. J., Wallace, D., Chintagumpala, M. M., Woo, S. Y., Ashley, D. M., Sexton, M., Kellie, S. J., Ahern, V., & Gajjar, A. (2008). Multi-institution prospective trial of reduced-dose craniospinal irradiation (23.4 Gy) followed by conformal posterior fossa (36 Gy) and primary site irradiation (55.8 Gy) and dose-intensive chemotherapy for average-risk medulloblastoma. International journal of radiation oncology, biology, physics, 70(3), 782–787. doi.org/10.1016/j.ijrobp.2007.07.2342.

Choi J. Y. (2023). Medulloblastoma: Current Perspectives and Recent Advances. *Brain tumor research and treatment*, *11*(1), 28–38. doi.org/10.14791/btrt.2022.0046.

Cavalli, F. M. G., Remke, M., Rampasek, L., Peacock, J., Shih, D. J. H., Luu, B., Garzia, L., Torchia, J., Nor, C., Morrissy, A. S., Agnihotri, S., Thompson, Y. Y., Kuzan-Fischer, C. M., Farooq, H.,

Isaev, K., Daniels, C., Cho, B. K., Kim, S. K., Wang, K. C., Lee, J. Y., … Taylor, M. D. (2017). Intertumoral Heterogeneity within Medulloblastoma Subgroups. Cancer cell, 31(6), 737–754.e6. doi.org/10.1016/j.ccell.2017.05.005.

Northcott, P. A., Buchhalter, I., Morrissy, A. S., Hovestadt, V., Weischenfeldt, J., Ehrenberger, T., Gröbner, S., Segura-Wang, M., Zichner, T., Rudneva, V. A., Warnatz, H. J., Sidiropoulos, N., Phillips, A. H., Schumacher, S., Kleinheinz, K., Waszak, S. M., Erkek, S., Jones, D. T. W., Worst, B. C., Kool, M., … Lichter, P. (2017). The whole-genome landscape of medulloblastoma subtypes. Nature, 547(7663), 311–317. doi.org/10.1038/nature22973.

Sharma, T., Schwalbe, E. C., Williamson, D., Sill, M., Hovestadt, V., Mynarek, M., Rutkowski, S., Robinson, G. W., Gajjar, A., Cavalli, F., Ramaswamy, V., Taylor, M. D., Lindsey, J. C., Hill, R. M., Jäger, N., Korshunov, A., Hicks, D., Bailey, S., Kool, M., Chavez, L., … Clifford, S. C. (2019). Second-generation molecular subgrouping of medulloblastoma: an international meta-analysis of Group 3 and Group 4 subtypes. Acta neuropathologica, 138(2), 309–326. doi.org/10.1007/s00401-019-02020-0.

Taylor, M. D., Northcott, P. A., Korshunov, A., Remke, M., Cho, Y. J., Clifford, S. C., Eberhart, C. G., Parsons, D. W., Rutkowski, S., Gajjar, A., Ellison, D. W., Lichter, P., Gilbertson, R. J., Pomeroy, S. L., Kool, M., & Pfister, S. M. (2012). Molecular subgroups of medulloblastoma: the current consensus. Acta neuropathologica, 123(4), 465–472. doi.org/10.1007/s00401-011-0922-z.

Godbole, S., Voß, H., Gocke, A., Schlumbohm, S., Schumann, Y., Peng, B., Mynarek, M., Rutkowski, S., Dottermusch, M., Dorostkar, M. M., Korshunov, A., Mair, T., Pfister, S. M., Kwiatkowski, M., Hotze, M., Neumann, P., Hartmann, C., Weis, J., Liesche-Starnecker, F., Guan, Y., … Neumann, J. E. (2024). Multiomic profiling of medulloblastoma reveals subtype-specific targetable alterations at the proteome and N-glycan level. Nature communications, 15(1), 6237. doi.org/10.1038/s41467-024-50554-z.

Forget, A., Martignetti, L., Puget, S., Calzone, L., Brabetz, S., Picard, D., Montagud, A., Liva, S., Sta, A., Dingli, F., Arras, G., Rivera, J., Loew, D., Besnard, A., Lacombe, J., Pagès, M., Varlet, P., Dufour, C., Yu, H., Mercier, A. L., … Ayrault, O. (2018). Aberrant ERBB4-SRC Signaling as a Hallmark of Group 4 Medulloblastoma Revealed by Integrative Phosphoproteomic Profiling. Cancer cell, 34(3), 379–395.e7. doi.org/10.1016/j.ccell.2018.08.002.

Thompson, M. C., Fuller, C., Hogg, T. L., Dalton, J., Finkelstein, D., Lau, C. C., Chintagumpala, M., Adesina, A., Ashley, D. M., Kellie, S. J., Taylor, M. D., Curran, T., Gajjar, A., & Gilbertson, R.

J. (2006). Genomics identifies medulloblastoma subgroups that are enriched for specific genetic alterations. *Journal of clinical oncology : official journal of the American Society of Clinical Oncology*, *24*(12), 1924–1931. doi.org/10.1200/JCO.2005.04.4974.

Northcott, P. A., Rutka, J. T., & Taylor, M. D. (2010). Genomics of medulloblastoma: from Giemsa-banding to next-generation sequencing in 20 years. Neurosurgical focus, 28(1), E6. doi.org/10.3171/2009.10.FOCUS09218.

Hovestadt, V., Ayrault, O., Swartling, F. J., Robinson, G. W., Pfister, S. M., & Northcott, P. A. (2020). Medulloblastomics revisited: biological and clinical insights from thousands of patients. *Nature reviews. Cancer*, *20*(1), 42–56. doi.org/10.1038/s41568-019-0223-8.

Cho, Y. J., Tsherniak, A., Tamayo, P., Santagata, S., Ligon, A., Greulich, H., Berhoukim, R., Amani, V., Goumnerova, L., Eberhart, C. G., Lau, C. C., Olson, J. M., Gilbertson, R. J., Gajjar, A., Delattre, O., Kool, M., Ligon, K., Meyerson, M., Mesirov, J. P., & Pomeroy, S. L. (2011). Integrative genomic analysis of medulloblastoma identifies a molecular subgroup that drives poor clinical outcome. *Journal of clinical oncology : official journal of the American Society of Clinical Oncology*, *29*(11), 1424–1430. doi.org/10.1200/JCO.2010.28.5148.

Northcott, P. A., Korshunov, A., Witt, H., Hielscher, T., Eberhart, C. G., Mack, S., Bouffet, E., Clifford, S. C., Hawkins, C. E., French, P., Rutka, J. T., Pfister, S., & Taylor, M. D. (2011). Medulloblastoma comprises four distinct molecular variants. *Journal of clinical oncology: official journal of the American Society of Clinical Oncology*, *29*(11), 1408–1414. doi.org/10.1200/JCO.2009.27.4324.

Ellison, D. W., Dalton, J., Kocak, M., Nicholson, S. L., Fraga, C., Neale, G., Kenney, A. M., Brat, D. J., Perry, A., Yong, W. H., Taylor, R. E., Bailey, S., Clifford, S. C., & Gilbertson, R. J. (2011). Medulloblastoma: clinicopathological correlates of SHH, WNT, and non-SHH/WNT molecular subgroups. Acta neuropathologica, 121(3), 381–396. doi.org/10.1007/s00401-011-0800-8.

Louis, D. N., Perry, A., Wesseling, P., Brat, D. J., Cree, I. A., Figarella-Branger, D., Hawkins, C., Ng, H. K., Pfister, S. M., Reifenberger, G., Soffietti, R., von Deimling, A., & Ellison, D. W. (2021). The 2021 WHO Classification of Tumors of the Central Nervous System: a summary. Neuro-oncology, 23(8), 1231–1251. doi.org/10.1093/neuonc/noab106.

Sturm, D., Capper, D., Andreiuolo, F., Gessi, M., Kölsche, C., Reinhardt, A., Sievers, P., Wefers, A. K., Ebrahimi, A., Suwala, A. K., Gielen, G. H., Sill, M., Schrimpf, D., Stichel, D., Hovestadt, V., Daenekas, B., Rode, A., Hamelmann, S., Previti, C., Jäger, N., … Jones, D. T. W. (2023).

Multiomic neuropathology improves diagnostic accuracy in pediatric neuro-oncology. *Nature medicine*, *29*(4), 917–926. doi.org/10.1038/s41591-023-02255-1.

Helgager, J., Pytel, P., Vasudevaraja, V., Lee, E. Q., Snuderl, M., Iorgulescu, J. B., & Ligon, K. L. (2020). WNT-Activated Medulloblastomas With Hybrid Molecular Subtypes. *JCO precision oncology*, *4*, PO.19.00332. doi.org/10.1200/PO.19.00332.

Kool, M., Korshunov, A., Remke, M., Jones, D. T., Schlanstein, M., Northcott, P. A., Cho, Y. J., Koster, J., Schouten-van Meeteren, A., van Vuurden, D., Clifford, S. C., Pietsch, T., von Bueren, A. O., Rutkowski, S., McCabe, M., Collins, V. P., Bäcklund, M. L., Haberler, C., Bourdeaut, F., Delattre, O., … Pfister, S. M. (2012). Molecular subgroups of medulloblastoma: an international meta-analysis of transcriptome, genetic aberrations, and clinical data of WNT, SHH, Group 3, and Group 4 medulloblastomas. *Acta neuropathologica*, *123*(4), 473–484. doi.org/10.1007/s00401-012-0958-8.

Phoenix, T. N., Patmore, D. M., Boop, S., Boulos, N., Jacus, M. O., Patel, Y. T., Roussel, M. F., Finkelstein, D., Goumnerova, L., Perreault, S., Wadhwa, E., Cho, Y. J., Stewart, C. F., & Gilbertson, R. J. (2016). Medulloblastoma Genotype Dictates Blood Brain Barrier Phenotype. *Cancer cell*, *29*(4), 508–522. doi.org/10.1016/j.ccell.2016.03.002.

Rogers, H. A., Miller, S., Lowe, J., Brundler, M. A., Coyle, B., & Grundy, R. G. (2009). An investigation of WNT pathway activation and association with survival in central nervous system primitive neuroectodermal tumours (CNS PNET). *British journal of cancer*, *100*(8), 1292–1302. doi.org/10.1038/sj.bjc.6604979.

Cadigan, K. M., & Waterman, M. L. (2012). TCF/LEFs and Wnt signaling in the nucleus. *Cold Spring Harbor perspectives in biology*, *4*(11), a007906. doi.org/10.1101/cshperspect.a007906.

Clifford, S. C., Lusher, M. E., Lindsey, J. C., Langdon, J. A., Gilbertson, R. J., Straughton, D., & Ellison, D. W. (2006). Wnt/Wingless pathway activation and chromosome 6 loss characterize a distinct molecular sub-group of medulloblastomas associated with a favorable prognosis. Cell cycle (Georgetown, Tex.), 5(22), 2666–2670. doi.org/10.4161/cc.5.22.3446.

Waszak, S. M., Northcott, P. A., Buchhalter, I., Robinson, G. W., Sutter, C., Groebner, S., Grund, K. B., Brugières, L., Jones, D. T. W., Pajtler, K. W., Morrissy, A. S., Kool, M., Sturm, D., Chavez, L., Ernst, A., Brabetz, S., Hain, M., Zichner, T., Segura-Wang, M., Weischenfeldt, J., … Pfister, S. M. (2018). Spectrum and prevalence of genetic predisposition in medulloblastoma: a

retrospective genetic study and prospective validation in a clinical trial cohort. *The Lancet. Oncology*, *19*(6), 785–798. doi.org/10.1016/S1470-2045(18)30242-0.

Goschzik, T., Mynarek, M., Doerner, E., Schenk, A., Spier, I., Warmuth-Metz, M., Bison, B., Obrecht, D., Struve, N., Kortmann, R. D., Schmid, M., Aretz, S., Rutkowski, S., & Pietsch, T. (2022). Genetic alterations of TP53 and OTX2 indicate increased risk of relapse in WNT medulloblastomas. *Acta neuropathologica*, *144*(6), 1143–1156. doi.org/10.1007/s00401-022-02505-5.

Hatten, M. E., & Heintz, N. (1995). Mechanisms of neural patterning and specification in the developing cerebellum. *Annual review of neuroscience*, *18*, 385–408. doi.org/10.1146/annurev.ne.18.030195.002125.

Rutkowski, S., von Hoff, K., Emser, A., Zwiener, I., Pietsch, T., Figarella-Branger, D., Giangaspero, F., Ellison, D. W., Garre, M. L., Biassoni, V., Grundy, R. G., Finlay, J. L., Dhall, G., Raquin, M. A., & Grill, J. (2010). Survival and prognostic factors of early childhood medulloblastoma: an international meta-analysis. *Journal of clinical oncology : official journal of the American Society of Clinical Oncology*, *28*(33), 4961–4968. doi.org/10.1200/JCO.2010.30.2299.

Louis, D. N., Ohgaki, H., Wiestler, O. D., Cavenee, W. K., Burger, P. C., Jouvet, A., Scheithauer, B. W., & Kleihues, P. (2007). The 2007 WHO classification of tumours of the central nervous system. *Acta neuropathologica*, *114*(2), 97–109. doi.org/10.1007/s00401-007-0243-4.

Northcott, P. A., Dubuc, A. M., Pfister, S., & Taylor, M. D. (2012). Molecular subgroups of medulloblastoma. *Expert review of neurotherapeutics*, *12*(7), 871–884. doi.org/10.1586/ern.12.66.

Wefers, A. K., Warmuth-Metz, M., Pöschl, J., von Bueren, A. O., Monoranu, C. M., Seelos, K., Peraud, A., Tonn, J. C., Koch, A., Pietsch, T., Herold-Mende, C., Mawrin, C., Schouten-van Meeteren, A., van Vuurden, D., von Hoff, K., Rutkowski, S., Pfister, S. M., Kool, M., & Schüller, U. (2014). Subgroup-specific localization of human medulloblastoma based on pre-operative MRI. Acta neuropathologica, 127(6), 931–933. doi.org/10.1007/s00401-014-1271-5.

Ohli, J., Neumann, J. E., Grammel, D., & Schüller, U. (2015). Localization of SHH medulloblastoma in mice depends on the age at its initiation. Acta neuropathologica, 130(2), 307–309. doi.org/10.1007/s00401-015-1453-9.

Wong, G. C., Li, K. K., Wang, W. W., Liu, A. P., Huang, Q. J., Chan, A. K., Poon, M. F., Chung, N.

Y., Wong, Q. H., Chen, H., Chan, D. T. M., Liu, X. Z., Mao, Y., Zhang, Z. Y., Shi, Z. F., & Ng, H. K. (2020). Clinical and mutational profiles of adult medulloblastoma groups. *Acta neuropathologica communications*, *8*(1), 191. doi.org/10.1186/s40478-020-01066-6.

Zhukova, N., Ramaswamy, V., Remke, M., Pfaff, E., Shih, D. J., Martin, D. C., Castelo-Branco, P., Baskin, B., Ray, P. N., Bouffet, E., von Bueren, A. O., Jones, D. T., Northcott, P. A., Kool, M., Sturm, D., Pugh, T. J., Pomeroy, S. L., Cho, Y. J., Pietsch, T., Gessi, M., … Tabori, U. (2013). Subgroup-specific prognostic implications of TP53 mutation in medulloblastoma. Journal of clinical oncology : official journal of the American Society of Clinical Oncology, 31(23), 2927–2935. doi.org/10.1200/JCO.2012.48.5052.

Schwalbe, E. C., Lindsey, J. C., Nakjang, S., Crosier, S., Smith, A. J., Hicks, D., Rafiee, G., Hill, R. M., Iliasova, A., Stone, T., Pizer, B., Michalski, A., Joshi, A., Wharton, S. B., Jacques, T. S., Bailey, S., Williamson, D., & Clifford, S. C. (2017). Novel molecular subgroups for clinical classification and outcome prediction in childhood medulloblastoma: a cohort study. *The Lancet. Oncology*, *18*(7), 958–971. doi.org/10.1016/S1470-2045(17)30243-7.

Robinson, G. W., Rudneva, V. A., Buchhalter, I., Billups, C. A., Waszak, S. M., Smith, K. S., Bowers, D. C., Bendel, A., Fisher, P. G., Partap, S., Crawford, J. R., Hassall, T., Indelicato, D. J., Boop, F., Klimo, P., Sabin, N. D., Patay, Z., Merchant, T. E., Stewart, C. F., Orr, B. A., … Northcott, P. A. (2018). Risk-adapted therapy for young children with medulloblastoma (SJYC07): therapeutic and molecular outcomes from a multicentre, phase 2 trial. *The Lancet. Oncology*, *19*(6), 768–784. doi.org/10.1016/S1470-2045(18)30204-3.

Cavalli, F. M. G., Remke, M., Rampasek, L., Peacock, J., Shih, D. J. H., Luu, B., Garzia, L., Torchia, J., Nor, C., Morrissy, A. S., Agnihotri, S., Thompson, Y. Y., Kuzan-Fischer, C. M., Farooq, H., Isaev, K., Daniels, C., Cho, B. K., Kim, S. K., Wang, K. C., Lee, J. Y., … Taylor, M. D. (2017). Intertumoral Heterogeneity within Medulloblastoma Subgroups. *Cancer cell*, *31*(6), 737–754.e6. doi.org/10.1016/j.ccell.2017.05.005.Raybaud, C., Ramaswamy, V., Taylor, M. D., & Laughlin, S. (2015). Posterior fossa tumors in children: developmental anatomy and diagnostic imaging. *Child's nervous system : ChNS : official journal of the International Society for Pediatric Neurosurgery*, *31*(10), 1661–1676. doi.org/10.1007/s00381-015-2834-z.

Pitolli, C., Marini, A., Guerra, M., Pieraccioli, M., Marabitti, V., Palluzzi, F., Giacò, L., Tamburrini, G., Cecconi, F., Nazio, F., Sette, C., & Pagliarini, V. (2023). MYC up-regulation confers vulnerability to dual inhibition of CDK12 and CDK13 in high-risk Group 3 medulloblastoma.

Journal of experimental & clinical cancer research : CR, *42*(1), 214. doi.org/10.1186/s13046-023-02790-2.

Northcott, P. A., Lee, C., Zichner, T., Stütz, A. M., Erkek, S., Kawauchi, D., Shih, D. J., Hovestadt, V., Zapatka, M., Sturm, D., Jones, D. T., Kool, M., Remke, M., Cavalli, F. M., Zuyderduyn, S., Bader, G. D., VandenBerg, S., Esparza, L. A., Ryzhova, M., Wang, W., … Pfister, S. M. (2014). Enhancer hijacking activates GFI1 family oncogenes in medulloblastoma. *Nature*, *511*(7510), 428–434. doi.org/10.1038/nature13379.

Northcott, P. A., Jones, D. T., Kool, M., Robinson, G. W., Gilbertson, R. J., Cho, Y. J., Pomeroy, S. L., Korshunov, A., Lichter, P., Taylor, M. D., & Pfister, S. M. (2012). Medulloblastomics: the end of the beginning. *Nature reviews. Cancer*, *12*(12), 818–834. doi.org/10.1038/nrc3410.

Shih, D. J., Northcott, P. A., Remke, M., Korshunov, A., Ramaswamy, V., Kool, M., Luu, B., Yao, Y., Wang, X., Dubuc, A. M., Garzia, L., Peacock, J., Mack, S. C., Wu, X., Rolider, A., Morrissy, A. S., Cavalli, F. M., Jones, D. T., Zitterbart, K., Faria, C. C., … Taylor, M. D. (2014). Cytogenetic prognostication within medulloblastoma subgroups. *Journal of clinical oncology : official journal of the American Society of Clinical Oncology*, *32*(9), 886–896. doi.org/10.1200/JCO.2013.50.9539.

Ntenti, C., Lallas, K., & Papazisis, G. (2023). Clinical, Histological, and Molecular Prognostic Factors in Childhood Medulloblastoma: Where Do We Stand?. *Diagnostics (Basel, Switzerland)*, *13*(11), 1915. doi.org/10.3390/diagnostics13111915.

Kijima, N., & Kanemura, Y. (2016). Molecular Classification of Medulloblastoma. *Neurologia medico-chirurgica*, *56*(11), 687–697. doi.org/10.2176/nmc.ra.2016-0016.

Kumar, R., Liu, A. P. Y., & Northcott, P. A. (2020). Medulloblastoma genomics in the modern molecular era. *Brain pathology (Zurich, Switzerland)*, *30*(3), 679–690. doi.org/10.1111/bpa.12804.

Skowron, P., Ramaswamy, V., & Taylor, M. D. (2015). Genetic and molecular alterations across medulloblastoma subgroups. *Journal of molecular medicine (Berlin, Germany)*, *93*(10), 1075–1084. doi.org/10.1007/s00109-015-1333-8.

Leitner, A., Joachimiak, L. A., Bracher, A., Mönkemeyer, L., Walzthoeni, T., Chen, B., Pechmann, S., Holmes, S., Cong, Y., Ma, B., Ludtke, S., Chiu, W., Hartl, F. U., Aebersold, R., & Frydman, J. (2012). The molecular architecture of the eukaryotic chaperonin TRiC/CCT. *Structure (London, England : 1993)*, *20*(5), 814–825. doi.org/10.1016/j.str.2012.03.007.

Yam, A. Y., Xia, Y., Lin, H. T., Burlingame, A., Gerstein, M., & Frydman, J. (2008). Defining the

TRiC/CCT interactome links chaperonin function to stabilization of newly made proteins with complex topologies. *Nature structural & molecular biology*, *15*(12), 1255–1262. doi.org/10.1038/nsmb.1515.

Sternlicht, H., Farr, G. W., Sternlicht, M. L., Driscoll, J. K., Willison, K., & Yaffe, M. B. (1993). The t-complex polypeptide 1 complex is a chaperonin for tubulin and actin in vivo. *Proceedings of the National Academy of Sciences of the United States of America*, *90*(20), 9422–9426. doi.org/10.1073/pnas.90.20.9422.

Vallin, J., Córdoba-Beldad, C. M., & Grantham, J. (2021). Sequestration of the Transcription Factor STAT3 by the Molecular Chaperone CCT: A Potential Mechanism for Modulation of STAT3 Phosphorylation. *Journal of molecular biology*, *433*(13), 166958. doi.org/10.1016/j.jmb.2021.166958.

Trinidad, A. G., Muller, P. A., Cuellar, J., Klejnot, M., Nobis, M., Valpuesta, J. M., & Vousden, K. H. (2013). Interaction of p53 with the CCT complex promotes protein folding and wild-type p53 activity. *Molecular cell*, *50*(6), 805–817. doi.org/10.1016/j.molcel.2013.05.002.

Camasses, A., Bogdanova, A., Shevchenko, A., & Zachariae, W. (2003). The CCT chaperonin promotes activation of the anaphase-promoting complex through the generation of functional Cdc20. *Molecular cell*, *12*(1), 87–100. doi.org/10.1016/s1097-2765(03)00244-2.

Meng, Y., Yang, L., Wei, X., Luo, H., Hu, Y., Tao, X., He, J., Zheng, X., Xu, Q., Luo, K., Yu, G., & Luo, Q. (2021). CCT5 interacts with cyclin D1 promoting lung adenocarcinoma cell migration and invasion. *Biochemical and biophysical research communications*, *567*, 222–229. doi.org/10.1016/j.bbrc.2021.04.105.

Yokota, S., Yanagi, H., Yura, T., & Kubota, H. (1999). Cytosolic chaperonin is up-regulated during cell growth. Preferential expression and binding to tubulin at G(1)/S transition through early S phase. *The Journal of biological chemistry*, *274*(52), 37070–37078. doi.org/10.1074/jbc.274.52.37070.

Zhao, M., Spiess, M., Johansson, H. J., Olofsson, H., Hu, J., Lehtiö, J., & Strömblad, S. (2017). Identification of the PAK4 interactome reveals PAK4 phosphorylation of N-WASP and promotion of Arp2/3-dependent actin polymerization. *Oncotarget*, *8*(44), 77061–77074. doi.org/10.18632/oncotarget.20352.

Spiess, M., Echbarthi, M., Svanström, A., Karlsson, R., & Grantham, J. (2015). Over-Expression Analysis of All Eight Subunits of the Molecular Chaperone CCT in Mammalian Cells Reveals

a Novel Function for CCTdelta. *Journal of molecular biology*, *427*(17), 2757–2764. doi.org/10.1016/j.jmb.2015.06.007.

Nomura, N., Miyajima, N., Sazuka, T., Tanaka, A., Kawarabayasi, Y., Sato, S., Nagase, T., Seki, N., Ishikawa, K., & Tabata, S. (1994). Prediction of the coding sequences of unidentified human genes. I. The coding sequences of 40 new genes (KIAA0001-KIAA0040) deduced by analysis of randomly sampled cDNA clones from human immature myeloid cell line KG-1. *DNA research : an international journal for rapid publication of reports on genes and genomes*, *1*(1), 27–35. doi.org/10.1093/dnares/1.1.27.

Liao, Q., Ren, Y., Yang, Y., Zhu, X., Zhi, Y., Zhang, Y., Chen, Y., Ding, Y., & Zhao, L. (2021). CCT8 recovers WTp53-suppressed cell cycle evolution and EMT to promote colorectal cancer progression. *Oncogenesis*, *10*(12), 84. doi.org/10.1038/s41389-021-00374-3.

Liu, P., Kong, L., Jin, H., Wu, Y., Tan, X., & Song, B. (2019). Differential secretome of pancreatic cancer cells in serum-containing conditioned medium reveals CCT8 as a new biomarker of pancreatic cancer invasion and metastasis. *Cancer cell international*, *19*, 262. doi.org/10.1186/s12935-019-0980-1.

Cho, H. J., Baek, G. O., Yoon, M. G., Ahn, H. R., Son, J. A., Kim, S. S., Cheong, J. Y., & Eun, J. W. (2021). Overexpressed Proteins in HCC Cell-Derived Exosomes, CCT8, and Cofilin-1 Are Potential Biomarkers for Patients with HCC. *Diagnostics (Basel, Switzerland)*, *11*(7), 1221. doi.org/10.3390/diagnostics11071221.

Liu, J., Huang, L., Zhu, Y., He, Y., Zhang, W., Lei, T., Xuan, J., Xiao, B., Li, L., Zhou, Q., & Sun, Z. (2021). Exploring the Expression and Prognostic Value of the TCP1 Ring Complex in Hepatocellular Carcinoma and Overexpressing Its Subunit 5 Promotes HCC Tumorigenesis. *Frontiers in oncology*, *11*, 739660. doi.org/10.3389/fonc.2021.739660.

Yin, H., Miao, X., Wu, Y., Wei, Y., Zong, G., Yang, S., Chen, X., Zheng, G., Zhu, X., Guo, Y., Li, C., Chen, Y., Wang, Y., & He, S. (2016). The role of the Chaperonin containing t-complex polypeptide 1, subunit 8 (CCT8) in B-cell non-Hodgkin's lymphoma. *Leukemia research*, *45*, 59–67. doi.org/10.1016/j.leukres.2016.04.010.

Qiu, X., He, X., Huang, Q., Liu, X., Sun, G., Guo, J., Yuan, D., Yang, L., Ban, N., Fan, S., Tao, T., & Wang, D. (2015). Overexpression of CCT8 and its significance for tumor cell proliferation, migration and invasion in glioma. *Pathology, research and practice*, *211*(10), 717–725. doi.org/10.1016/j.prp.2015.04.012.

Prados M. D. (2023). Current Strategies for Management of Medulloblastoma. Diagnostics

(Basel, Switzerland), 13(16), 2622. doi.org/10.3390/diagnostics13162622.

Subramanian S, Ahmad T. Childhood Brain Tumors. [Updated 2023 Aug 8]. In: StatPearls [Internet]. Treasure Island (FL): StatPearls Publishing; 2024 Jan-. Available from: https://www.ncbi.nlm.nih.gov/books/NBK535415/

Lutz, K., Jünger, S. T., & Messing-Jünger, M. (2022). Essential Management of Pediatric Brain Tumors. *Children (Basel, Switzerland)*, *9*(4), 498. doi.org/10.3390/children9040498.

Ozair, A., Khan, E., Bhat, V., Faruqi, A., & Nanda, A. (2022). Pediatric Brain Tumors: From Modern Classification System to Current Principles of Management. IntechOpen. doi: 10.5772/intechopen.100442

Krist, D. T., Naik, A., Thompson, C. M., Kwok, S. S., Janbahan, M., Olivero, W. C., & Hassaneen, W. (2022). Management of brain metastasis. Surgical resection versus stereotactic radiotherapy: a meta-analysis. Neuro-oncology advances, 4(1), vdac033. doi.org/10.1093/noajnl/vdac033.

Cooney, T., Lindsay, H., Leary, S., & Wechsler-Reya, R. (2023). Current studies and future directions for medulloblastoma: A review from the pacific pediatric neuro-oncology consortium (PNOC) disease working group. Neoplasia (New York, N.Y.), 35, 100861. doi.org/10.1016/j.neo.2022.100861.

Wang, Y. X., Wu, H., Ren, Y., Lv, S., Ji, C., Xiang, D., Zhang, M., Lu, H., Fu, W., Liu, Q., Yan, Z., Ma, Q., Miao, J., Cai, R., Lan, X., Wu, B., Wang, W., Liu, Y., Wang, D. Z., Cao, M., … Bian, X. W. (2022). Elevated Kir2.1/nuclear N2ICD defines a highly malignant subtype of non-WNT/SHH medulloblastomas. Signal transduction and targeted therapy, 7(1), 72. doi.org/10.1038/s41392-022-00890-7.

Nishimura, T., & Akiyoshi, K. (2020). Artificial Molecular Chaperone Systems for Proteins, Nucleic Acids, and Synthetic Molecules. Bioconjugate chemistry, 31(5), 1259–1267. doi.org/10.1021/acs.bioconjchem.0c00133.

Bhattacharya, A., & Chatterji, U. (2024). Exosomal misfolded proteins released by cancer stem cells: dual functions in balancing protein homeostasis and orchestrating tumor progression. Discover oncology, 15(1), 392. doi.org/10.1007/s12672-024-01262-z.

Rinauro, D. J., Chiti, F., Vendruscolo, M., & Limbocker, R. (2024). Misfolded protein oligomers: mechanisms of formation, cytotoxic effects, and pharmacological approaches against protein misfolding diseases. Molecular neurodegeneration, 19(1), 20. doi.org/10.1186/s13024-023-00651-2.

Que, Y., Qiu, Y., Ding, Z., Zhang, S., Wei, R., Xia, J., & Lin, Y. (2024). The role of molecular chaperone CCT/TRiC in translation elongation: A literature review. Heliyon, 10(7), e29029. doi.org/10.1016/j.heliyon.2024.e29029.

Smith, T. M., & Willardson, B. M. (2022). Mechanistic insights into protein folding by the eukaryotic chaperonin complex CCT. Biochemical Society transactions, 50(5), 1403–1414. doi.org/10.1042/BST20220591.

Lv, W., Shi, L., Pan, J., & Wang, S. (2022). Comprehensive prognostic and immunological analysis of CCT2 in pan-cancer. Frontiers in oncology, 12, 986990. doi.org/10.3389/fonc.2022.986990.

Novikov, N. M., Zolotaryova, S. Y., Gautreau, A. M., & Denisov, E. V. (2021). Mutational drivers of cancer cell migration and invasion. British journal of cancer, 124(1), 102–114. doi.org/10.1038/s41416-020-01149-0.

Svanström, A., & Grantham, J. (2016). The molecular chaperone CCT modulates the activity of the actin filament severing and capping protein gelsolin in vitro. Cell stress & chaperones, 21(1), 55–62. doi.org/10.1007/s12192-015-0637-5.

Zeng, C., Han, S., Pan, Y., Huang, Z., Zhang, B., & Zhang, B. (2024). Revisiting the chaperonin T-complex protein-1 ring complex in human health and disease: A proteostasis modulator and beyond. Clinical and translational medicine, 14(2), e1592. doi.org/10.1002/ctm2.1592.

Liao, Q., Ren, Y., Yang, Y., Zhu, X., Zhi, Y., Zhang, Y., Chen, Y., Ding, Y., & Zhao, L. (2021). CCT8 recovers WTp53-suppressed cell cycle evolution and EMT to promote colorectal cancer progression. Oncogenesis, 10(12), 84. doi.org/10.1038/s41389-021-00374-3.

Wang, Y., Gong, X., & Zhang, Y. (2021). Network-based approach to identify prognosis-related genes in tamoxifen-treated patients with estrogen receptor-positive breast cancer. Bioscience reports, 41(9), BSR20203020. doi.org/10.1042/BSR20203020.

Zaytseva, O., Kim, N. H., & Quinn, L. M. (2020). MYC in Brain Development and Cancer. International journal of molecular sciences, 21(20), 7742. doi.org/10.3390/ijms21207742.

Roussel, M. F., & Robinson, G. W. (2013). Role of MYC in Medulloblastoma. Cold Spring Harbor perspectives in medicine, 3(11), a014308. doi.org/10.1101/cshperspect.a014308.

Zheng, L., Chen, X., Zhang, L., Qin, N., An, J., Zhu, J., Jin, H., & Tuo, B. (2023). A potential tumor marker: Chaperonin containing TCP-1 controls the development of malignant tumors (Review). International journal of oncology, 63(3), 106. doi.org/10.3892/ijo.2023.5554.

Banyal, A., Tiwari, S., Sharma, A., Chanana, I., Patel, S. K. S., Kulshrestha, S., & Kumar, P. (2023). Vinca alkaloids as a potential cancer therapeutics: recent update and future challenges. 3 Biotech, 13(6), 211. doi.org/10.1007/s13205-023-03636-6.

8. Abbreviations

Abbreviations	Full name
AA	Amino acid
AB	Antibody
ACN	Acetonitrile
AGC	Automatic gain control
ATCC	American Type Culture Collection
ANOVA	Analysis of Variance
ASD	Alternative Splicing Database
ATP	Adenosine triphosphate
BLAST	Basic Local Alignment Search Tool
BBB	Blood-brain barrier
BCA	Bicinchoninic acid
bp	Base pair
BSA	Bovine serum albumin
CCT	Chaperonin containing tailless complex polypeptide 1
CDK2	Cyclin-dependent kinases 2
CNS	Central nervous system
Cryo-SEM	Cryo-scanning electron microscopy
CTG	CellTiter-Glo
CRC	Colorectal Carcinoma
CTL	Cytotoxic T lymphocyte
CSI	Craniospinal irradiation
DDA	Data dependent acquisition
DMEM	Dulbecco's Modified Eagle Medium
DMSO	Dimethyl sulfoxide
DN	Desmoplastic /nodular
EB	Ethidium bromide
EBI	European Bioinformatics Institute
EM	Ependymoma
EMEM	Eagle's Minimal Essential Medium
EST	Expressed Sequence Tag
FA	Formic acid
FBS	Fetal Bovine Serum
FCS	fetal calf serum
FSTL5	Follistatin-related protein 5
GAPDH	Glyceraldehyde-3-phosphate dehydrogenase

GBM	Glioblastoma
GNPs	Granule neuron precursors
GTS	Genetic tumor syndromes
HCD	Higher energy collisional dissociation
HP	Hewlett-Packard
IDH	Isocitrate dehydrogenase
KDa	Kilodalton
LC	Liquid chromatography
LC/A	large cell /anaplastic
LSD	Least—Significant Difference
MB	Medullablastoma
MBEN	Medulloblastoma with extensive nodularity
min	Minute
miRNA	MicroRNA
MMPs	Matrix metalloproteinases
MS	Mass spectrometry
MS/MS	Tandem mass spectrometry
MSE	Mean Squared Error
nano-ESI	nano-electrospray ionization source
NCBI	National Center for Biotechnology Information
OD	Optical density
PAK4	p21-activated protein kinase 4
PVDF	Polyvinylidene fluoride
PBS	Phosphate-buffered saline
PCNA	Proliferating cell nuclear antigen
PFA	Paraformaldehyde
PH	Potential of hydrogen
RIPA	Radioimmunoprecipitation assay
RPMI	Roswell Park Memorial Institute
rmp	Revolutions per minute
RT	Room temperature
SAGE	Serial Analysis of Gene
SDC	Sodiumdeoxycholate
SDS-PAGE	sodium dodecyl sulfate polyacrylamide gel electrophoresis
SHH	Sonic Hedgehog
SNF	Similarity network fusion
STAT3	Signal transducer and activator of transcription 3
TAA	Tumor-associated antigen
TBS	Tris buffered saline

TEAB	Triethylammoniumbicarbonate
TRiC	T-complex protein Ring Complex
UKE	Universitätsklinikum Hamburg-Eppendorf
VHL	von Hippel-Lindau
WHO	World health organism
WT	Wild type

9. Figures

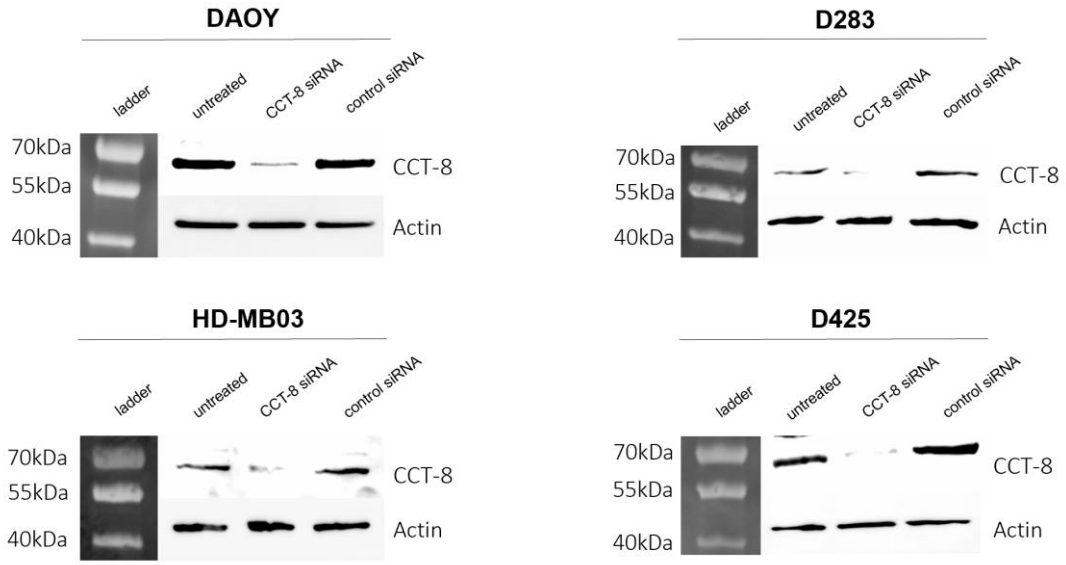

Figure 1. CCT-8 was knocked down in DAOY, D283, HD-MB03, and D425 cell lines. Representative Western blots of proteins from untreated cells, CCT-8 knockdown cells (CCT-8 siRNA), and control cells (non-target control siRNA) are shown.

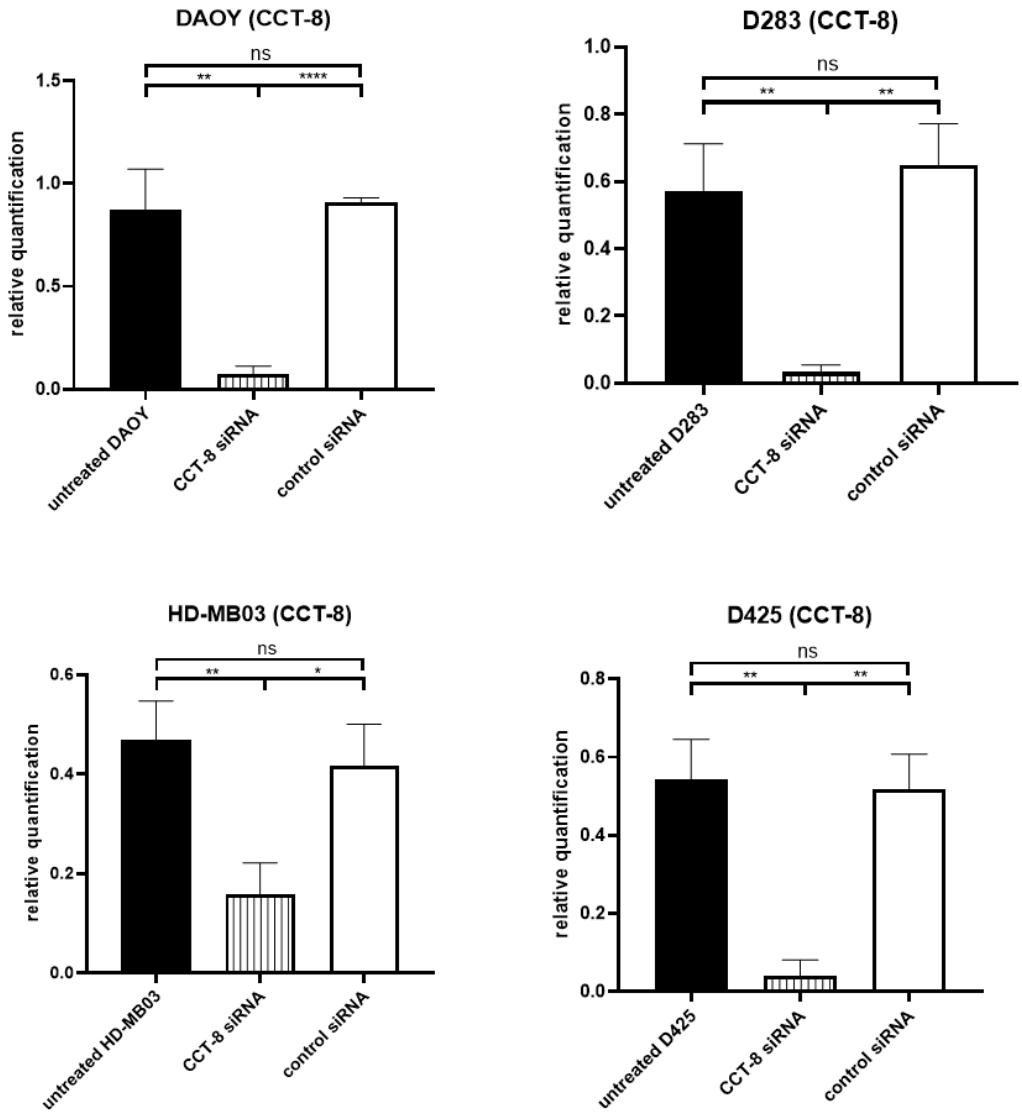

*Figure 2. Quantification of Western Blot experiments (n=3). Data were normalized to total protein as described in the methods. *p-value <0.05, **p-value <0.01, ***p-value <0.001, ****p-value <0.0001. ns, non-significant.*

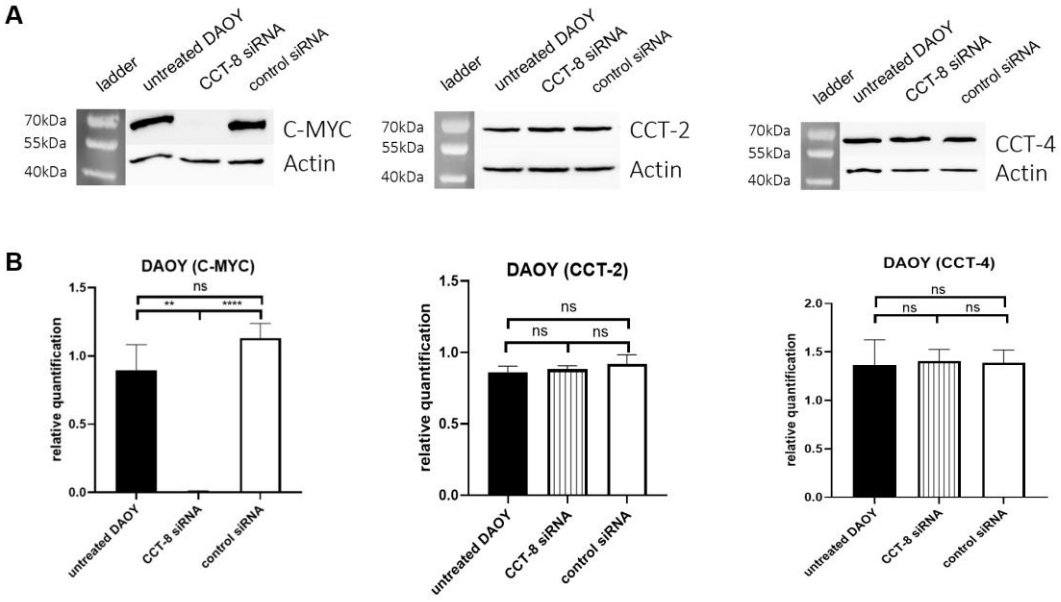

*Figure 3. Expression of C-MYC, CCT-2, and CCT-4 in the DAOY cell line after CCT-8 knockdown. (A) Representative Western blots of proteins from untreated cells, CCT-8 knockdown cells, and control cells are shown, respectively. The data have been normalized to total protein as described in the methods. (B) Quantification of Western Blot experiments (n=3). *p-value <0.05, **p-value <0.01, ***p-value <0.001, ****p-value <0.0001. ns, non-significant.*

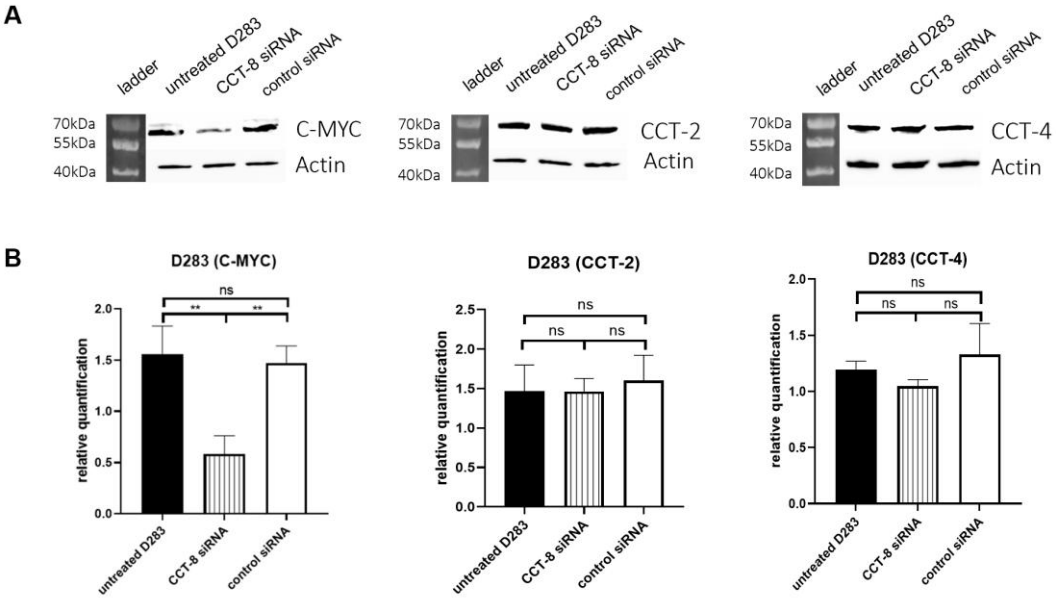

*Figure 4. Expression of C-MYC, CCT-2, and CCT-4 in the D283 cell line after CCT-8 knockdown. (A) Representative Western blots of proteins from untreated cells, CCT-8 knockdown cells, and control cells are shown, respectively. The data have been normalized to total protein as described in the methods. (B) Quantification of Western Blot experiments (n=3). *p-value <0.05, **p-value <0.01, ***p-value <0.001, ****p-value <0.0001. ns, non-significant.*

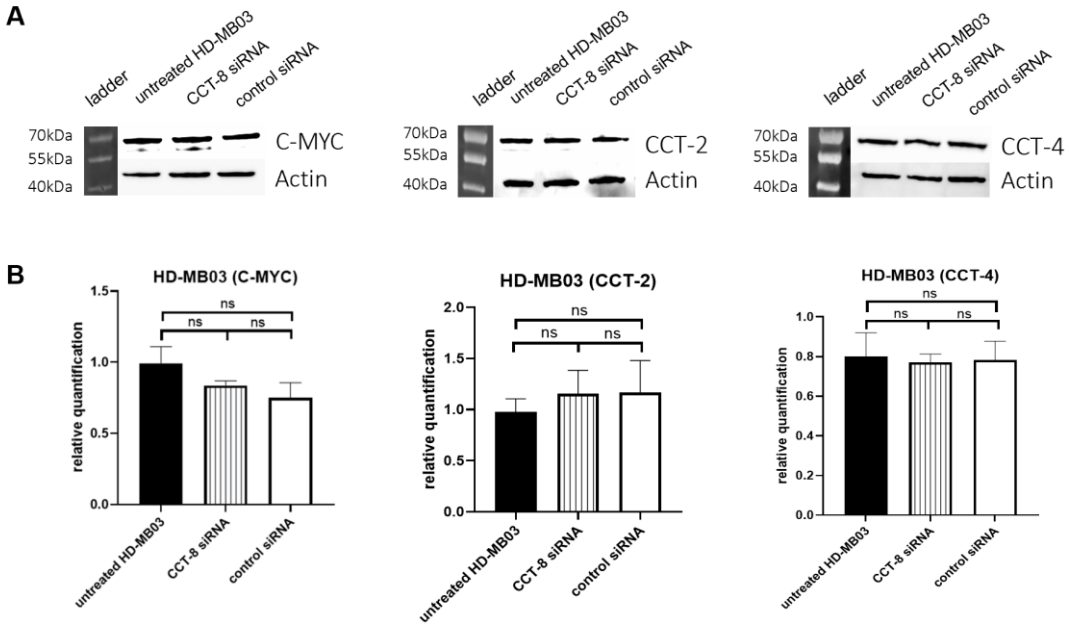

*Figure 5. Expression of C-MYC, CCT-2, and CCT-4 in HD-MB03 cell line after CCT-8 knockdown. (A) Representative Western blots of proteins from untreated cells, CCT-8 knockdown cells, and control cells are shown, respectively. The data have been normalized to total protein as described in the methods. (B) Quantification of Western Blot experiments (n=3). *p-value <0.05, **p-value <0.01, ***p-value <0.001, ****p-value <0.0001. ns, non-significant.*

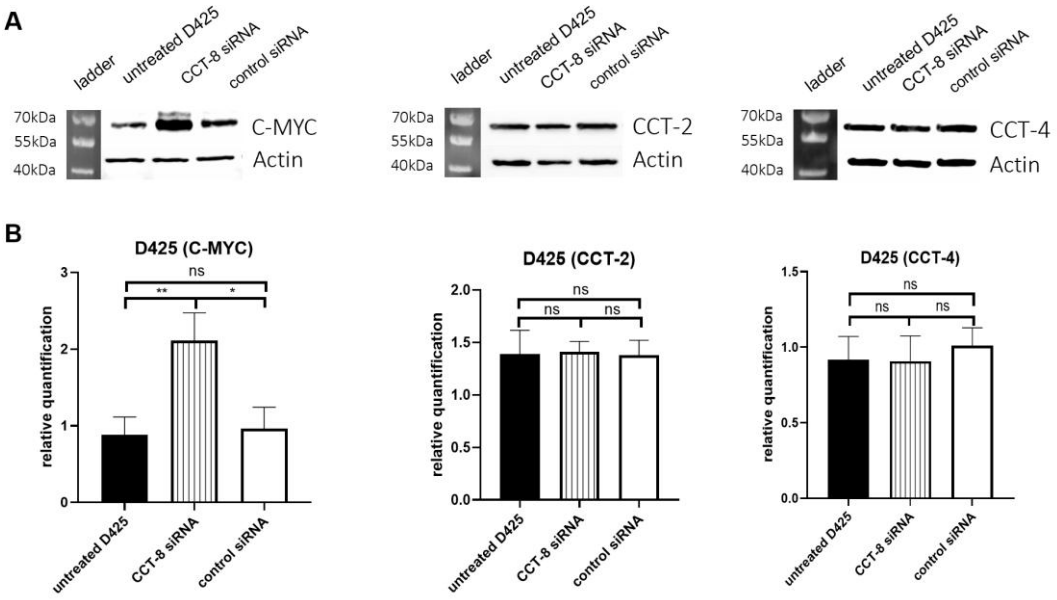

*Figure 6. Expression of C-MYC, CCT-2, and CCT-4 in the D425 cell line after CCT-8 knockdown. (A) Representative Western blots of proteins from untreated cells, CCT-8 knockdown cells, and control cells are shown, respectively. The data have been normalized to total protein as described in the methods. (B) Quantification of Western Blot experiments (n=3). *p-value <0.05, **p-value <0.01, ***p-value <0.001, ****p-value <0.0001. ns, non-significant.*

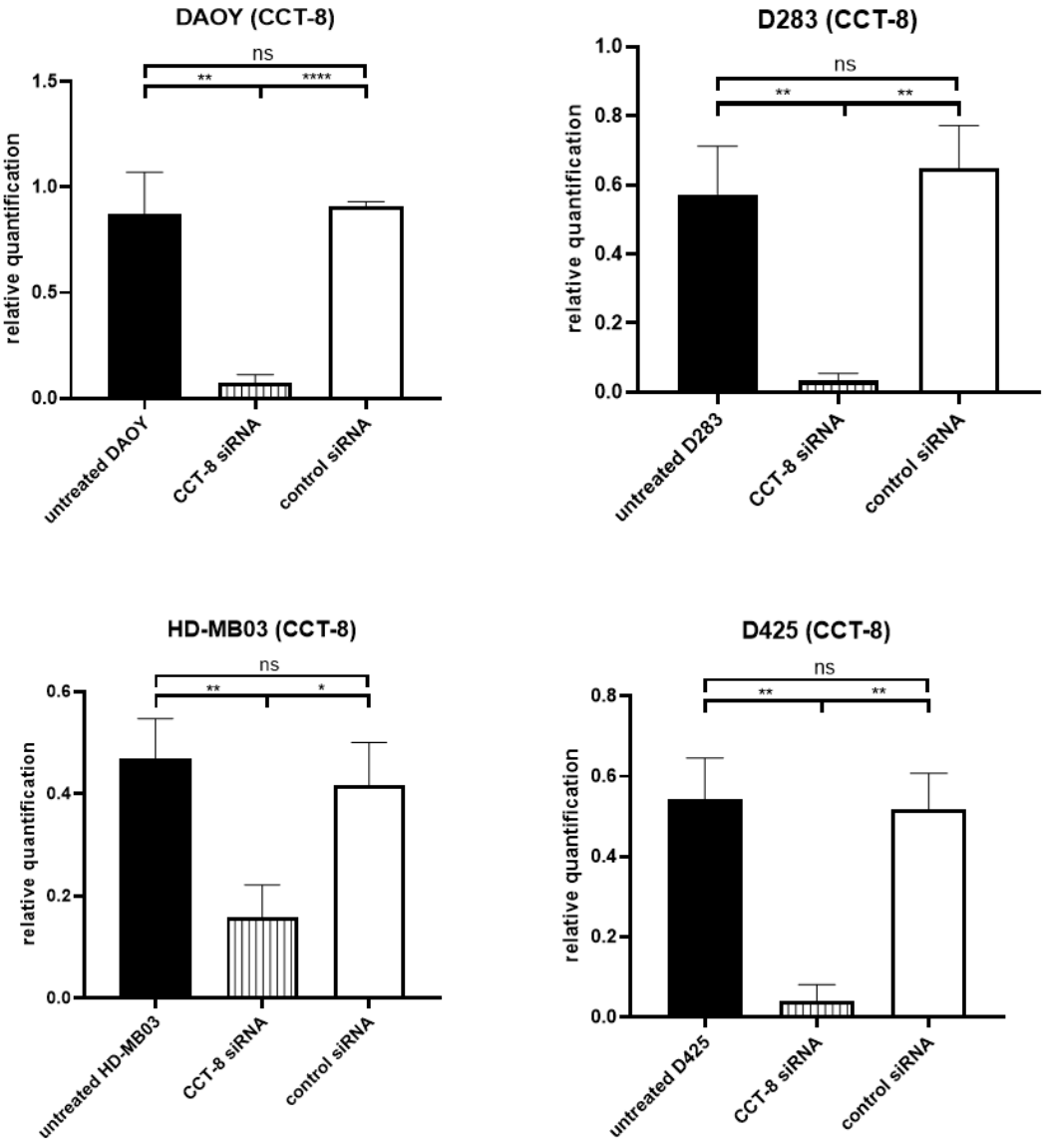

*Figure 7. Proliferation assay of medulloblastoma cells after CCT-8 knockdown (n=3 experiments shown for each cell line). In the DAOY cell line, the proliferation ability of CCT-8 knockdown cells was significantly reduced compared with the untreated cells (P＜0.01) and with the control group (P＜0.0001). In the D283 cell line, the proliferation ability of CCT-8 knockdown cells was significantly reduced compared with the untreated cells (P＜ 0.01) and compared with the control group (P＜0.01). In the HD-MB03 cell line, the proliferation ability of CCT-8 knockout cells was significantly reduced compared with the untreated cell (P＜0.01) and compared with the control group (P＜0.05). In the D425 cell line, the proliferation ability of CCT-8 knockdown cells was significantly reduced compared with the untreated cells (P < 0.01); and compared with the control group (P < 0.01). * p-value <0.05, **p-value <0.01, ****p-value <0.0001. ns, non-significant.*

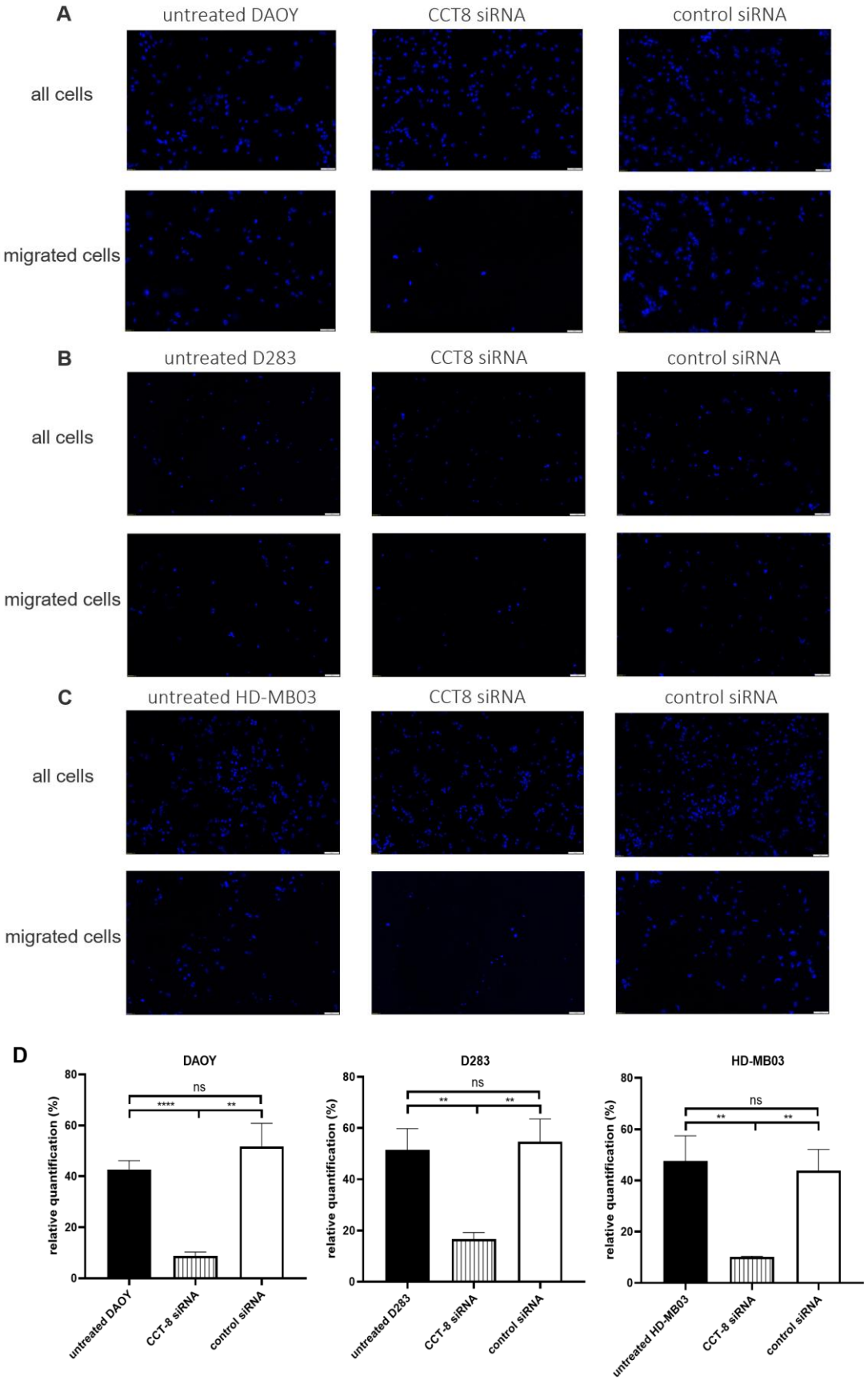
A
untreated DAOY
CCT8 siRNA
control siRNA
all cells
migrated cells
B
untreated D283
CCT8 siRNA
control siRNA
all cells
migrated cells
C
untreated HD-MB03
CCT8 siRNA
control siRNA
all cells
migrated cells
D
DAOY
D283
HD-MB03
relative quantification (%)
ns
****
**
untreated DAOY
CCT-8 siRNA
control siRNA
untreated D283
untreated HD-MB03

*Figure 8. Migration ability of medulloblastoma cell lines (n=3 experiments performed for each cell line). (A) DAOY cell line (B) D283 cell line (C) HD-MB03 cell line. The images represent show all cells stained with Hoechst and the number of cells present after removal of non-migrated cells (hence representing the fraction of migrated cells). The scale bar in the image corresponds to 100µm. (D) Compared with the untreated and control groups, the migration abilities of DAOY cells, D283 cells and HD-MB03 cells were significantly reduced after CCT-8 knockdown. * p-value <0.05, **p-value <0.01, ****p-value <0.0001. ns, non-significant.*

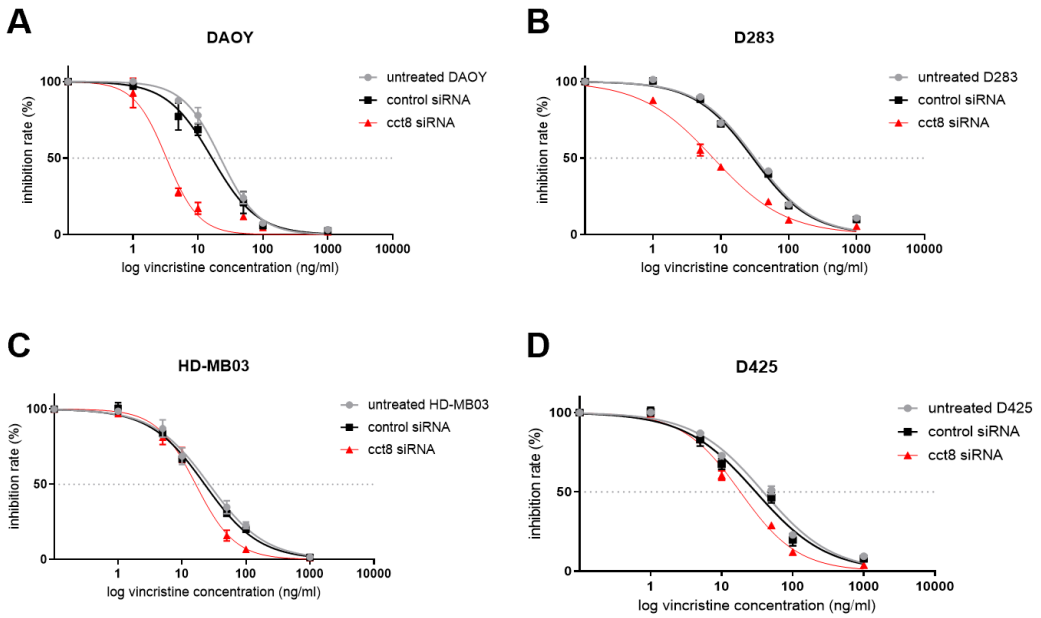

Figure 9. Dose-response curves displaying the effect of increasing concentrations of Vincristine on medulloblastoma cells, comparing cells with CCT-8 knockdown (in red) with untreated (grey) and control transfected medulloblastoma cells (black, n=3 experiments for each cell line). IC-50 was used to evaluate drug sensitivity. (A) DAOY cell line. The values of IC-50 for untreated, CCT-8 knockdown, and control transfected medulloblastoma cells are 22.20, 3.272, and 16.42, respectively. (B) D283 cell line. The values of IC-50 for untreated, CCT-8 knockdown, and control transfected medulloblastoma cells are 31.83, 7.757, and 29.68, respectively. (C) HD-MB03 cell line. The values of IC-50 for untreated, CCT-8 knockdown, and control transfected medulloblastoma cells are 26.47, 16.37, and 22.59, respectively. (D) D425 cell line. The values of IC-50 for untreated, CCT-8 knockdown, and control transfected medulloblastoma cells are 38.45, 18.24, and 30.17, respectively.

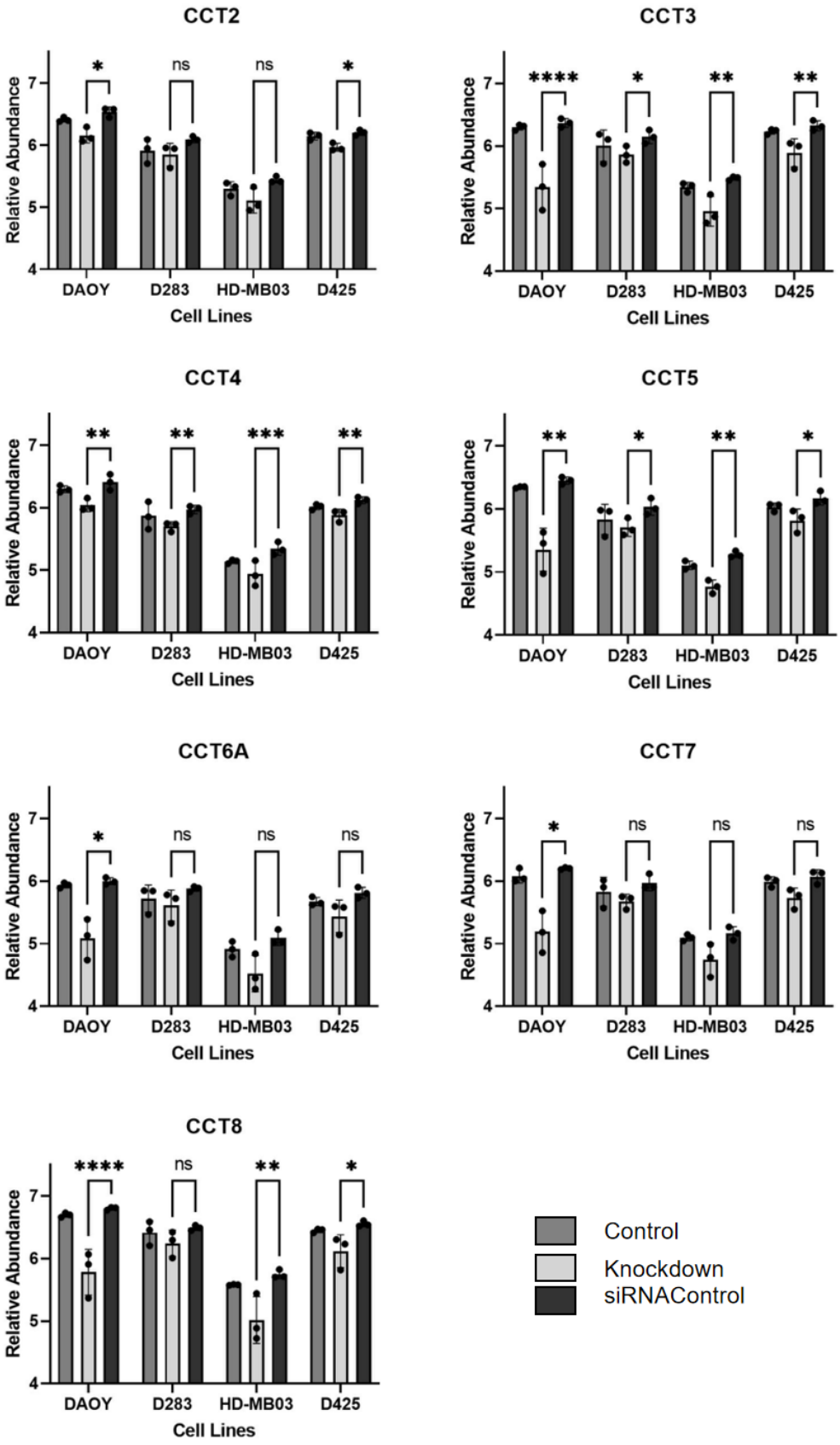

*Figure 10. Relative protein abundances of the CCT components measured using mass spectrometry (n=3). *p-value <0.05, **p-value <0.01, ***p-value <0.001, ****p-value <0.0001. ns, non-significant.*

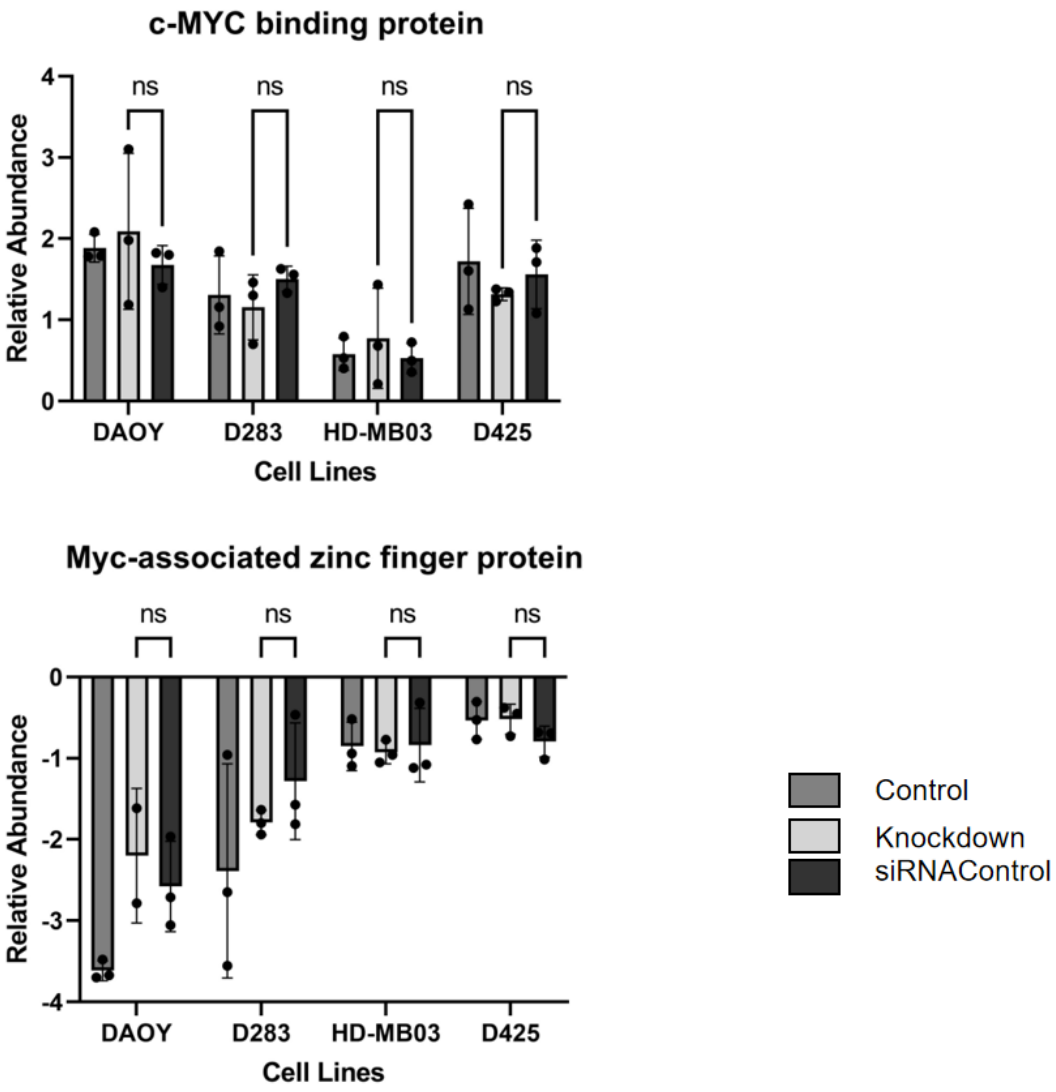

*Figure 11. Relative protein abundances of the C-MYC associated proteins measured using mass spectrometry (n=3). *p-value <0.05, **p-value <0.01, ***p-value <0.001, ****p-value <0.0001. ns, non-significant.*

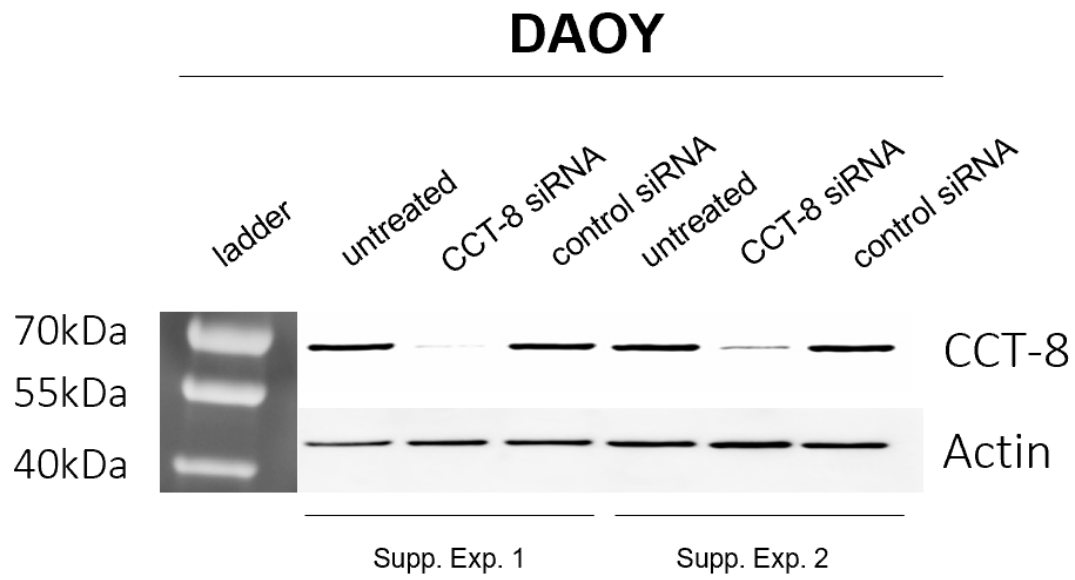

Supplementary Figure 1 related to Figure 1. Western blots of supplementary experiment (Supp. Exp.) 1 and 2 in DAOY cell line.

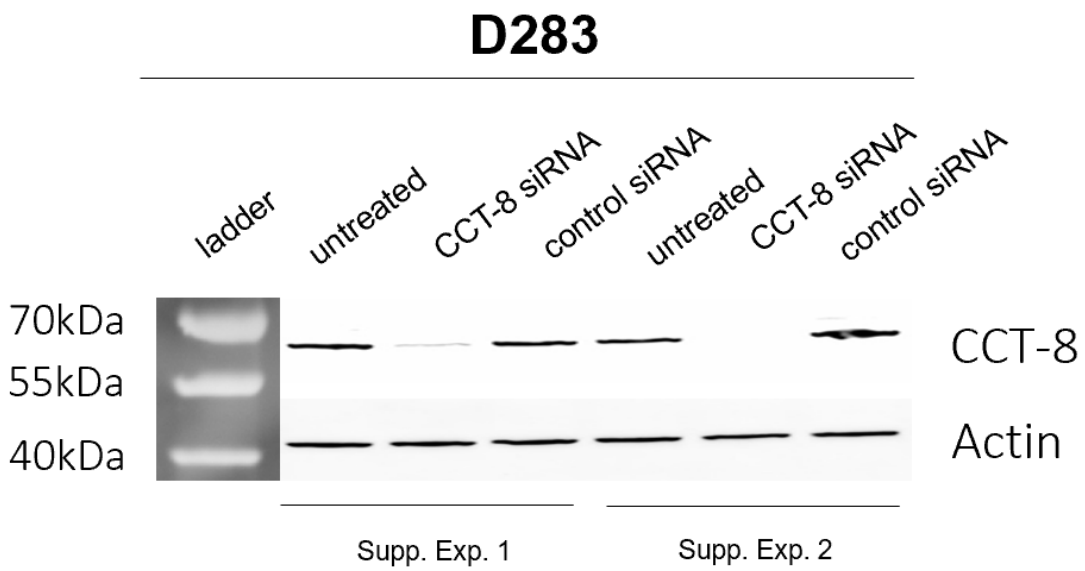

Supplementary Figure 2 related to Figure 1. Supplementary Figure 1 related to Figure 1. Western blots of supplementary experiment (Supp. Exp.) 1 and 2 in D283 cell line.

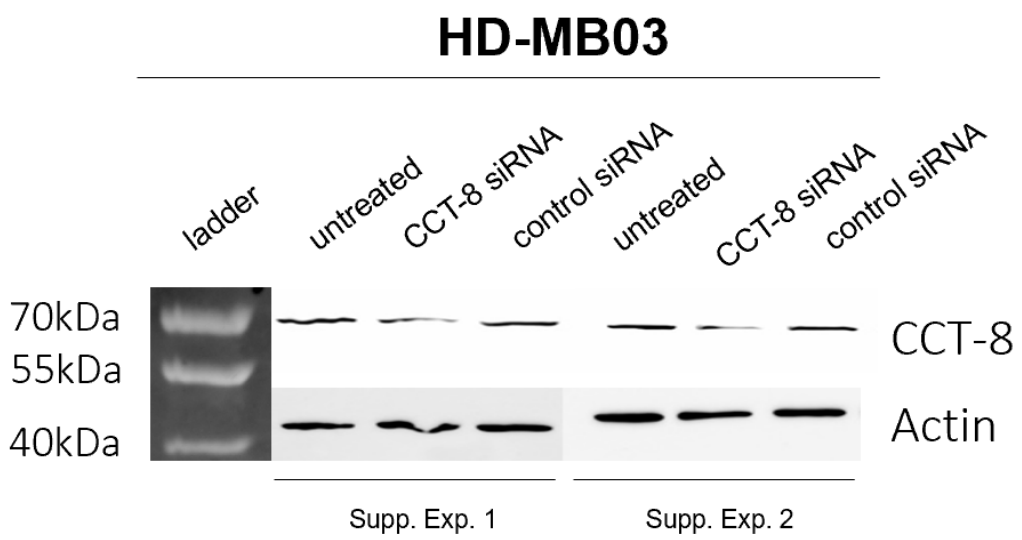

Supplementary Figure 3 related to Figure 1. Supplementary Figure 1 related to Figure 1. Western blots of supplementary experiment (Supp. Exp.) 1 and 2 in HD-MB03 cell line.

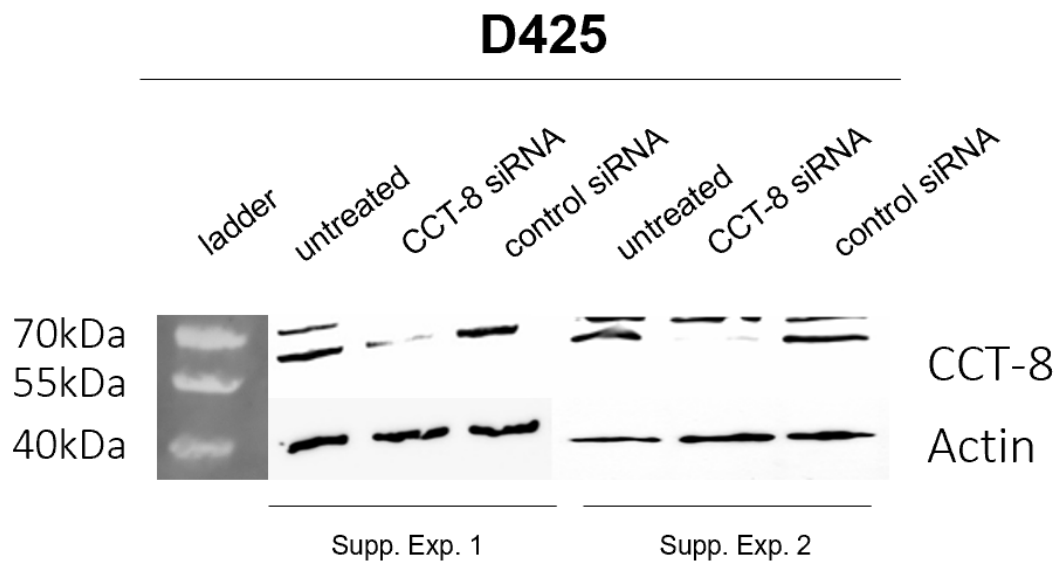

Supplementary Figure 4 related to Figure 1. Supplementary Figure 1 related to Figure 1. Western blots of supplementary experiment (Supp. Exp.) 1 and 2 in D425 cell line.

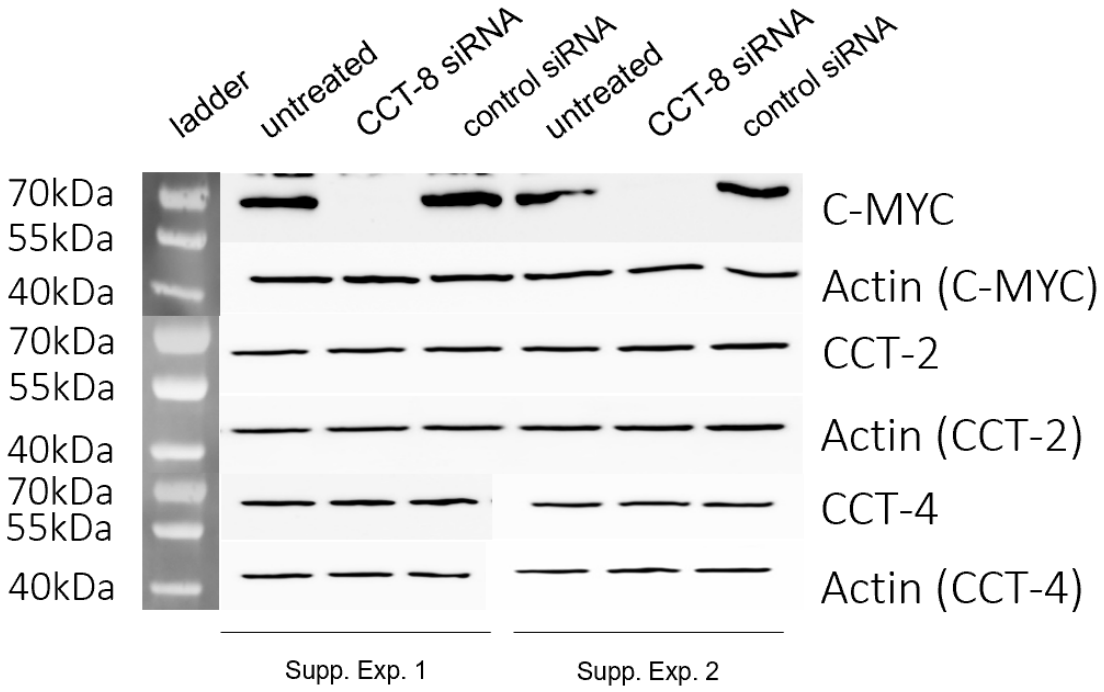

Supplementary Figure 5 related to Figure 3. Expression of C-MYC, CCT-2, and CCT-4 in DAOY cell line after CCT-8 knockdown. Western blots of proteins from untreated cells, CCT-8 knockdown cells, and control cells are shown, respectively.

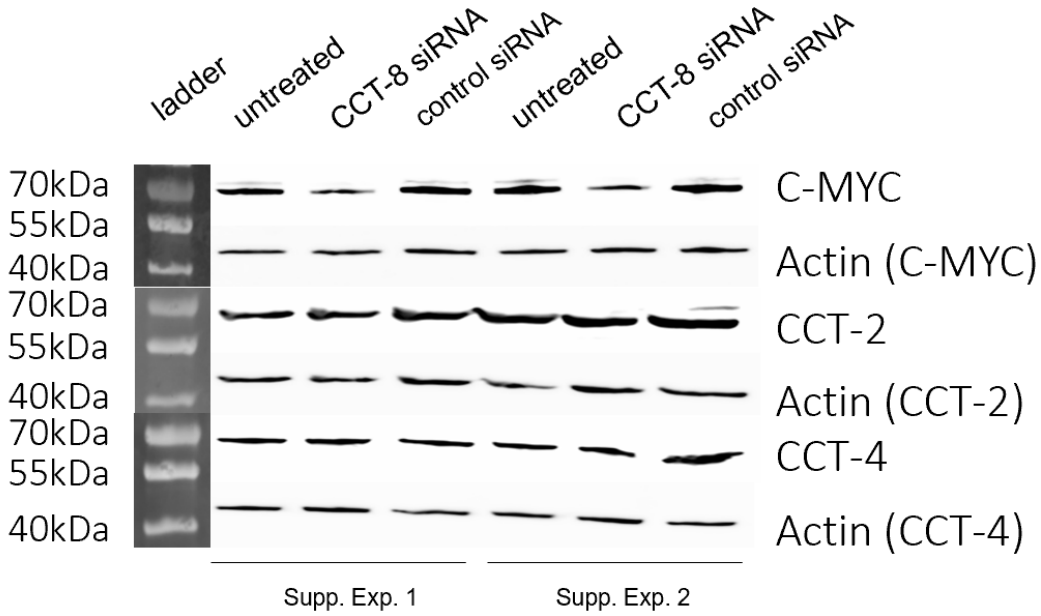

Supplementary Figure 6 related to Figure 4. Expression of C-MYC, CCT-2, and CCT-4 in D283 cell line after CCT-8 knockdown. Western blots of proteins from untreated cells, CCT-8 knockdown cells, and control cells are shown, respectively.

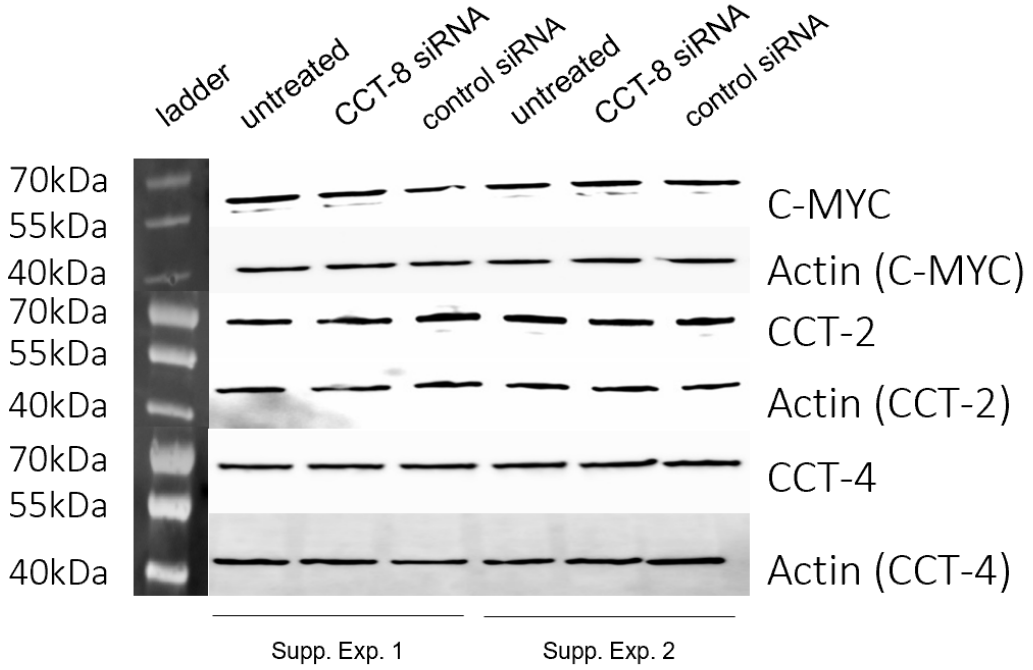

Supplementary Figure 7 related to Figure 5. Expression of C-MYC, CCT-2, and CCT-4 in HD-MB03 cell line after CCT-8 knockdown. Western blots of proteins from untreated cells, CCT-8 knockdown cells, and control cells are shown, respectively.

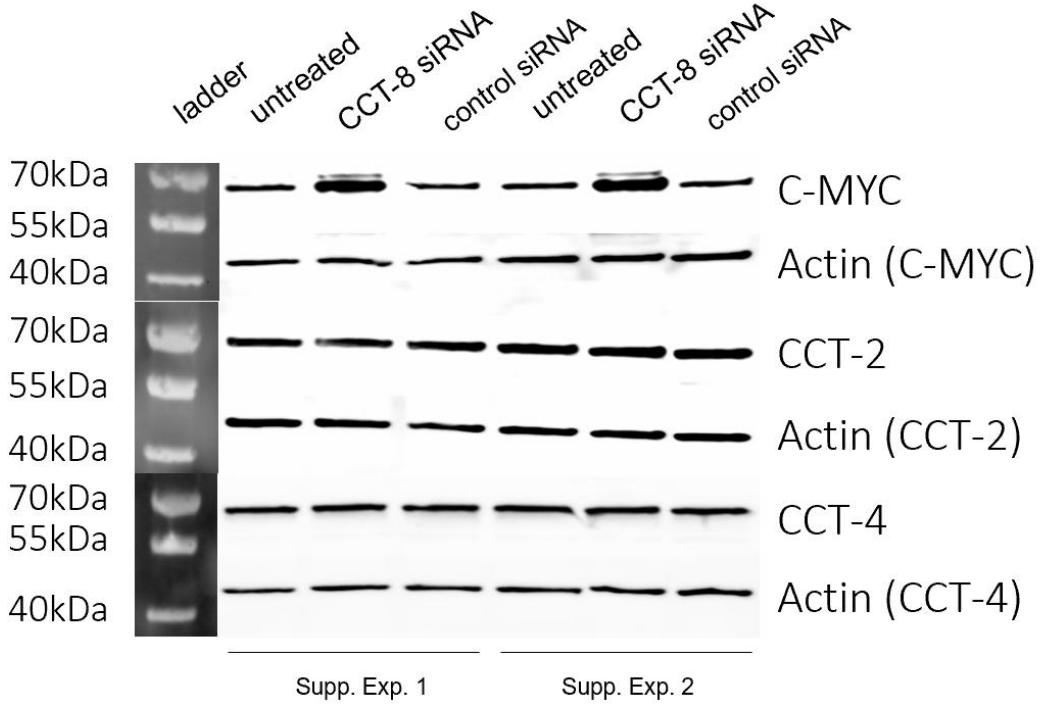

Supplementary Figure 8 related to Figure 6. Expression of C-MYC, CCT-2, and CCT-4 in D425 cell line after CCT-8 knockdown. Western blots of proteins from untreated cells, CCT-8 knockdown cells, and control cells are shown, respectively.

10. Tables

Name	Experiment 1			Experiment 2			Experiment 3		
DAOY	Untreated DAOY	CCT-8 siRNA	Control siRNA	Untreated DAOY	CCT-8 siRNA	Control siRNA	Untreated DAOY	CCT-8 siRNA	Control siRNA
CCT-8	1.37E+05	1.55E+04	1.46E+05	1.44E+05	4.55E+03	1.43E+05	1.55E+05	2.13E+04	1.57E+05
C-MYC	1.67E+05	9.65E+02	2.07E+05	1.23E+05	1.68E+03	1.41E+05	1.66E+05	1.55E+03	1.72E+05
CCT-2	1.13E+05	1.39E+05	1.39E+05	1.25E+05	1.30E+05	1.39E+05	1.36E+05	1.53E+05	1.62E+05
CCT-4	1.77E+05	1.70E+05	1.78E+05	1.72E+05	1.69E+05	1.40E+05	1.75E+05	1.69E+05	1.67E+05
Actin (CCT-8)	2.03E+05	1.92E+05	1.57E+05	1.34E+05	1.50E+05	1.56E+05	1.80E+05	1.96E+05	1.77E+05
Actin (C-MYC)	1.85E+05	1.86E+05	1.93E+05	1.78E+05	1.42E+05	1.32E+05	1.54E+05	1.32E+05	1.37E+05
Actin (CCT-2)	1.34E+05	1.59E+05	1.40E+05	1.38E+05	1.51E+05	1.57E+05	1.65E+05	1.68E+05	1.84E+05
Actin (CCT-4)	1.46E+05	1.33E+05	1.21E+05	1.42E+05	1.19E+05	1.13E+05	1.05E+05	1.11E+05	1.15E+05

Supplementary Table 1 related to Figure 2 and 3. Use grayscale analysis to digitize Western Blot bands in DAOY cell line. The results of biological replicate experiments are shown in the table.

Name	Experiment 1			Experiment 2			Experiment 3		
D283	Untreated D283	CCT-8 siRNA	Control siRNA	Untreated D283	CCT-8 siRNA	Control siRNA	Untreated D283	CCT-8 siRNA	Control siRNA
CCT-8	8.25E+04	7.52E+03	1.12E+05	1.07E+05	7.79E+03	9.43E+04	8.31E+04	1.21E+03	1.15E+05
C-MYC	2.39E+05	7.52E+04	2.19E+05	2.01E+05	9.99E+04	2.62E+05	2.57E+05	1.08E+05	2.82E+05
CCT-2	2.09E+05	1.93E+05	2.40E+05	2.01E+05	2.19E+05	2.78E+05	3.00E+05	3.19E+05	3.36E+05
CCT-4	1.95E+05	2.14E+05	1.96E+05	1.96E+05	2.06E+05	2.03E+05	1.81E+05	1.80E+05	2.30E+05
Actin (CCT-8)	1.93E+05	2.01E+05	2.08E+05	1.51E+05	1.50E+05	1.51E+05	1.43E+05	1.34E+05	1.42E+05
Actin (C-MYC)	1.92E+05	1.97E+05	1.69E+05	1.22E+05	1.40E+05	1.76E+05	1.45E+05	1.64E+05	1.73E+05
Actin (CCT-2)	1.55E+05	1.51E+05	1.67E+05	1.66E+05	1.40E+05	2.00E+05	1.63E+05	2.06E+05	1.70E+05
Actin (CCT-4)	1.75E+05	1.96E+05	1.92E+05	1.57E+05	1.92E+05	1.45E+05	1.48E+05	1.83E+05	1.47E+05

Supplementary Table 2 related to Figure 2 and 4. Use grayscale analysis to digitize Western Blot bands in D283 cell line. The results of biological replicate experiments are shown in the table.

Name	Experiment 1			Experiment 2			Experiment 3		
HD-MB03	Untreated HD-MB03	CCT-8 siRNA	Control siRNA	Untreated HD-MB03	CCT-8 siRNA	Control siRNA	Untreated HD-MB03	CCT-8 siRNA	Control siRNA
CCT-8	1.00E+05	4.30E+04	8.18E+04	9.89E+04	2.03E+04	1.08E+05	9.83E+04	3.49E+04	8.69E+04
C-MYC	1.46E+05	1.14E+05	7.72E+04	1.03E+05	1.24E+05	1.20E+05	1.45E+05	1.52E+05	1.26E+05
CCT-2	2.14E+05	2.38E+05	2.24E+05	1.65E+05	1.98E+05	2.34E+05	1.89E+05	1.89E+05	1.88E+05
CCT-4	1.74E+05	1.38E+05	1.74E+05	1.63E+05	1.68E+05	1.72E+05	1.73E+05	1.91E+05	1.97E+05
Actin (CCT-8)	1.89E+05	1.95E+05	2.20E+05	2.01E+05	2.22E+05	2.10E+05	2.59E+05	2.19E+05	2.39E+05
Actin (C-MYC)	1.43E+05	1.38E+05	1.20E+05	1.20E+05	1.42E+05	1.41E+05	1.33E+05	1.87E+05	1.66E+05
Actin (CCT-2)	2.32E+05	2.68E+05	2.74E+05	1.86E+05	1.50E+05	1.64E+05	1.68E+05	1.51E+05	1.50E+05
Actin (CCT-4)	1.92E+05	1.72E+05	2.33E+05	2.42E+05	2.31E+05	1.94E+05	2.11E+05	2.42E+05	2.78E+05

Supplementary Table 3 related to Figure 2 and 5. Use grayscale analysis to digitize Western Blot bands in HD-MB03 cell line. The results of biological replicate experiments are shown in the table.

Name	Experiment 1			Experiment 2			Experiment 3		
D425	Untreated D425	CCT-8 siRNA	Control siRNA	Untreated D425	CCT-8 siRNA	Control siRNA	Untreated D425	CCT-8 siRNA	Control siRNA
CCT-8	1.29E+05	2.28E+04	1.26E+05	8.25E+04	3.34E+03	8.96E+04	6.97E+04	3.29E+03	1.01E+05
C-MYC	9.82E+04	3.02E+05	1.59E+05	1.49E+05	3.05E+05	1.30E+05	1.61E+05	3.40E+05	1.50E+05
CCT-2	2.37E+05	2.04E+05	2.67E+05	2.11E+05	2.23E+05	2.28E+05	2.44E+05	2.36E+05	2.33E+05
CCT-4	2.34E+05	2.13E+05	2.65E+05	2.33E+05	2.14E+05	2.63E+05	2.87E+05	2.80E+05	2.81E+05
Actin (CCT-8)	2.31E+05	2.60E+05	2.52E+05	1.30E+05	2.31E+05	2.07E+05	1.61E+05	1.88E+05	1.65E+05
Actin (C-MYC)	1.39E+05	1.25E+05	1.31E+05	1.30E+05	1.38E+05	1.28E+05	2.04E+05	1.99E+05	2.27E+05
Actin (CCT-2)	2.06E+05	1.34E+05	1.83E+05	1.32E+05	1.66E+05	1.56E+05	1.72E+05	1.73E+05	1.93E+05
Actin (CCT-4)	2.98E+05	2.81E+05	3.00E+05	2.64E+05	2.44E+05	2.36E+05	2.64E+05	2.57E+05	2.72E+05

Supplementary Table 4 related to Figure 2 and 6. Use grayscale analysis to digitize Western Blot bands in D425 cell line. The results of biological replicate experiments are shown in the table.

DAOY	Untreated DAOY				CCT8 siRNA				Control siRNA			
Blank	1.07E+04	1.75E+04	1.81E+04	1.86E+04	1.29E+04	1.06E+04	1.04E+04	5.22E+03	1.98E+04	1.88E+04	1.94E+04	1.84E+04
Exp. 1	3.72E+07	3.28E+07	3.60E+07	3.72E+07	2.00E+07	1.73E+07	1.92E+07	1.50E+07	3.93E+07	3.77E+07	3.41E+07	3.64E+07
Exp. 2	3.18E+07	3.94E+07	3.28E+07	4.22E+07	1.83E+07	1.38E+07	1.98E+07	1.21E+07	3.42E+07	4.03E+07	3.74E+07	4.01E+07
Exp. 3	3.67E+07	3.58E+07	3.55E+07	3.36E+07	2.09E+07	2.19E+07	1.84E+07	1.76E+07	3.98E+07	3.39E+07	4.07E+07	3.45E+07

Supplementary Table 5 related to Figure 7. Quantification of adenosine triphosphate (ATP) to determine viable cell number and cell viability in DAOY cell line. The results of biological replicate experiments are shown in the table.

D283	Untreated D283				CCT8 siRNA				Control siRNA			
Blank	7.87E+03	1.23E+04	1.30E+04	1.22E+04	1.02E+04	1.00E+04	9.04E+03	5.67E+03	1.19E+04	1.19E+04	1.17E+04	1.02E+04
Exp. 1	2.31E+07	2.36E+07	2.39E+07	2.34E+07	1.75E+07	1.71E+07	1.71E+07	1.54E+07	2.37E+07	2.23E+07	2.28E+07	2.23E+07
Exp. 2	2.30E+07	2.54E+07	2.33E+07	2.62E+07	1.77E+07	1.81E+07	1.68E+07	1.62E+07	2.40E+07	2.17E+07	2.35E+07	2.40E+07
Exp. 3	2.28E+07	2.54E+07	2.33E+07	2.41E+07	1.65E+07	1.67E+07	1.72E+07	1.56E+07	2.19E+07	2.56E+07	2.35E+07	2.23E+07

Supplementary Table 6 related to Figure 7. Quantification of adenosine triphosphate (ATP) to determine viable cell number and cell viability in D283 cell line. The results of biological replicate experiments are shown in the table.

HD-MB03	Untreated HD-MB03				CCT8 siRNA				Control siRNA			
Blank	6.49E+03	1.02E+04	1.02E+04	1.04E+04	8.81E+03	7.55E+03	6.85E+03	4.03E+03	1.17E+04	1.09E+04	1.24E+04	1.23E+04
Exp. 1	2.38E+07	1.72E+07	2.11E+07	1.75E+07	1.35E+07	1.36E+07	1.12E+07	1.18E+07	2.56E+07	1.68E+07	2.49E+07	2.17E+07
Exp. 2	1.88E+07	2.30E+07	1.91E+07	2.61E+07	1.29E+07	1.42E+07	1.26E+07	1.16E+07	1.84E+07	2.27E+07	2.03E+07	1.80E+07
Exp. 3	2.43E+07	2.15E+07	2.46E+07	2.06E+07	1.18E+07	1.15E+07	1.38E+07	1.26E+07	2.00E+07	1.98E+07	2.43E+07	2.62E+07

Supplementary Table 7 related to Figure 7. Quantification of adenosine triphosphate (ATP) to determine viable cell number and cell viability in HD-MB03 cell line. The results of biological replicate experiments are shown in the table.

D425	Untreated D425				CCT8 siRNA				Control siRNA			
Blank	3.35E+03	5.27E+03	5.24E+03	4.62E+03	3.40E+03	2.55E+03	2.40E+03	1.53E+03	5.35E+03	5.47E+03	5.86E+03	5.35E+03
Exp. 1	1.03E+07	1.02E+07	9.68E+06	8.87E+06	4.36E+06	4.07E+06	3.93E+06	3.77E+06	9.23E+06	1.08E+07	9.53E+06	1.10E+07
Exp. 2	8.89E+06	1.03E+07	1.20E+07	1.06E+07	3.67E+06	4.89E+06	3.82E+06	3.49E+06	1.15E+07	9.77E+06	1.11E+07	1.15E+07
Exp. 3	1.03E+07	1.12E+07	1.03E+07	1.20E+07	4.32E+06	4.33E+06	4.63E+06	3.62E+06	1.04E+07	1.19E+07	1.02E+07	1.24E+07

Supplementary Table 8 related to Figure 7. Quantification of adenosine triphosphate (ATP) to determine viable cell number and cell viability in D425 cell lines. The results of biological replicate experiments are shown in the table.

Name	Before migration			After migration		
DAOY	Untreated DAOY	CCT-8 siRNA	Control siRNA	Untreated DAOY	CCT-8 siRNA	Control siRNA
Exp. 1	213	243	345	87	22	210
Exp. 2	198	350	357	81	25	184
Exp. 3	195	251	393	91	26	168

Supplementary Table 9 related to Figure 8. Count the number of cells before and after migration in DAOY cell line. The area of the measured pictures is 1.5 x 1.0 ㎜. The results of biological replicate experiments are shown in the table.

Name	Before migration			After migration		
D283	Untreated DAOY	CCT-8 siRNA	Control siRNA	Untreated DAOY	CCT-8 siRNA	Control siRNA
Exp. 1	149	121	195	91	18	90
Exp. 2	138	134	175	67	20	95
Exp. 3	174	109	160	78	21	102

Supplementary Table 10 related to Figure 8. Count the number of cells before and after migration in D283 cell line. The area of the measured pictures is 1.5 x 1.0 ㎜. The results of biological replicate experiments are shown in the table.

Name	Before migration			After migration		
HD-MB03	Untreated DAOY	CCT-8 siRNA	Control siRNA	Untreated DAOY	CCT-8 siRNA	Control siRNA
Exp. 1	367	345	408	133	36	159
Exp. 2	320	303	324	167	31	173
Exp. 3	266	333	474	144	33	186

Supplementary Table 11 related to Figure 8. Count the number of cells before and after migration in HD-MB03 cell line. The area of the measured pictures is 1.5 x 1.0 ㎜. The results of biological replicate experiments are shown in the table.

Exp.1	Untreated DAOY				CCT-8 siRNA				Control siRNA			
Blank	1.52E+03	1.90E+03	2.26E+03	1.93E+03	1.64E+03	1.54E+03	1.44E+03	1.08E+03	2.21E+03	1.94E+03	2.06E+03	1.94E+03
solvent	1.18E+07	1.24E+07	1.29E+07	1.29E+07	7.92E+06	8.19E+06	7.44E+06	6.87E+06	1.22E+07	1.19E+07	1.19E+07	1.19E+07
1ng/ml	1.28E+07	1.25E+07	1.29E+07	1.25E+07	8.12E+06	7.76E+06	8.04E+06	6.70E+06	1.20E+07	1.21E+07	1.20E+07	9.94E+06
5ng/ml	1.17E+07	1.10E+07	1.08E+07	1.14E+07	2.21E+06	1.80E+06	2.83E+06	1.79E+06	9.83E+06	9.14E+06	9.22E+06	8.14E+06
10ng/ml	1.05E+07	1.01E+07	9.92E+06	9.94E+06	1.53E+06	1.15E+06	1.06E+06	9.10E+05	8.07E+06	8.23E+06	7.63E+06	6.80E+06
50ng/ml	1.88E+06	3.36E+06	2.37E+06	2.19E+06	1.01E+06	8.91E+05	6.87E+05	6.50E+05	2.32E+06	1.88E+06	1.89E+06	1.68E+06
100ng/ml	7.07E+05	8.77E+05	8.48E+05	7.23E+05	3.39E+05	2.27E+05	2.59E+05	2.82E+05	5.63E+05	5.34E+05	5.59E+05	5.41E+05
1000ng/ml	3.10E+05	3.98E+05	3.55E+05	3.82E+05	1.02E+05	1.02E+05	1.00E+05	9.03E+04	2.70E+05	2.32E+05	1.96E+05	2.02E+05

Supplementary Table 12 related to Figure 9 (A). Quantification of adenosine triphosphate (ATP) to determine resistance of DAOY cell line to varying concentrations of vincristine. The results of biological replicate experiments are shown in the tables.

Exp.2	Untreated DAOY				CCT-8 siRNA				Control siRNA			
Blank	2.01E+03	2.31E+03	2.28E+03	2.14E+03	1.63E+03	1.54E+03	1.48E+03	1.18E+03	1.93E+03	1.98E+03	1.81E+03	1.76E+03
solvent	1.33E+07	1.36E+07	1.43E+07	1.35E+07	8.32E+06	8.37E+06	8.74E+06	7.17E+06	1.17E+07	1.16E+07	1.18E+07	1.15E+07
1ng/ml	1.30E+07	1.45E+07	1.36E+07	1.34E+07	7.70E+06	7.48E+06	6.32E+06	5.17E+06	1.16E+07	1.18E+07	1.18E+07	1.09E+07
5ng/ml	1.15E+07	1.18E+07	1.18E+07	1.20E+07	1.99E+06	2.51E+06	1.71E+06	1.97E+06	9.38E+06	6.72E+06	7.45E+06	8.56E+06
10ng/ml	9.86E+06	1.11E+07	1.05E+07	7.86E+06	1.36E+06	1.20E+06	1.15E+06	1.06E+06	9.18E+06	8.11E+06	8.10E+06	7.85E+06
50ng/ml	2.88E+06	3.34E+06	3.71E+06	4.28E+06	9.92E+05	1.07E+06	8.89E+05	7.51E+05	2.66E+06	2.01E+06	1.74E+06	1.71E+06
100ng/ml	1.05E+06	1.10E+06	1.31E+06	9.63E+05	3.99E+05	4.44E+05	4.13E+05	3.04E+05	7.66E+05	7.68E+05	5.70E+05	6.53E+05
1000ng/ml	4.41E+05	5.92E+05	4.29E+05	4.53E+05	1.20E+05	1.22E+05	1.23E+05	1.06E+05	3.09E+05	2.99E+05	2.95E+05	2.99E+05

Supplementary Table 13 related to Figure 9 (A). Quantification of adenosine triphosphate (ATP) to determine resistance of DAOY cell line to varying concentrations of vincristine. The results of biological replicate experiments are shown in the tables.

Exp.3	Untreated DAOY				CCT-8 siRNA				Control siRNA			
Blank	1.79E+03	2.25E+03	2.27E+03	2.31E+03	1.76E+03	1.65E+03	1.35E+03	1.14E+03	2.06E+03	2.11E+03	1.96E+03	1.90E+03
solvent	1.33E+07	1.36E+07	1.34E+07	1.32E+07	8.50E+06	8.24E+06	7.71E+06	6.86E+06	1.29E+07	1.28E+07	1.24E+07	1.21E+07
1ng/ml	1.29E+07	1.35E+07	1.35E+07	1.34E+07	8.64E+06	7.81E+06	7.12E+06	6.20E+06	1.26E+07	1.27E+07	1.09E+07	1.21E+07
5ng/ml	1.14E+07	1.13E+07	1.16E+07	1.21E+07	3.49E+06	2.57E+06	1.83E+06	1.50E+06	1.06E+07	1.13E+07	1.09E+07	1.06E+07
10ng/ml	1.01E+07	1.09E+07	1.12E+07	1.11E+07	2.61E+06	1.78E+06	1.24E+06	1.13E+06	7.73E+06	9.81E+06	9.02E+06	8.61E+06
50ng/ml	2.25E+06	3.46E+06	3.35E+06	5.07E+06	1.38E+06	1.30E+06	9.12E+05	7.03E+05	3.27E+06	3.92E+06	3.77E+06	3.64E+06
100ng/ml	9.78E+05	1.21E+06	1.09E+06	1.14E+06	5.78E+05	4.83E+05	4.06E+05	3.24E+05	8.63E+05	1.08E+06	7.47E+05	8.52E+05
1000ng/ml	3.44E+05	3.91E+05	5.09E+05	5.56E+05	2.23E+05	2.17E+05	2.02E+05	1.61E+05	4.11E+05	3.53E+05	3.20E+05	3.40E+05

Supplementary Table 14 related to Figure 9 (A). Supplementary Table 12 to 14 related to Figure 6 (A). Quantification of adenosine triphosphate (ATP) to determine resistance of DAOY cell line to varying concentrations of vincristine. The results of biological replicate experiments are shown in the tables.

Exp.1	Untreated D283				CCT-8 siRNA				Control siRNA			
Blank	2.04E+03	2.57E+03	2.63E+03	2.66E+03	2.10E+03	1.92E+03	1.91E+03	1.69E+03	2.27E+03	2.31E+03	2.34E+03	2.43E+03
solvent	1.59E+07	1.62E+07	1.63E+07	1.65E+07	1.09E+07	1.08E+07	1.10E+07	1.06E+07	1.49E+07	1.53E+07	1.52E+07	1.50E+07
1ng/ml	1.61E+07	1.67E+07	1.63E+07	1.64E+07	9.43E+06	9.73E+06	9.51E+06	9.08E+06	1.49E+07	1.50E+07	1.55E+07	1.46E+07
5ng/ml	1.45E+07	1.42E+07	1.45E+07	1.47E+07	5.98E+06	5.44E+06	5.28E+06	5.31E+06	1.33E+07	1.33E+07	1.35E+07	1.34E+07
10ng/ml	1.20E+07	1.22E+07	1.19E+07	1.19E+07	4.61E+06	4.74E+06	4.78E+06	4.49E+06	1.11E+07	1.12E+07	1.09E+07	1.09E+07
50ng/ml	6.77E+06	6.76E+06	6.80E+06	6.70E+06	2.18E+06	2.40E+06	2.28E+06	2.13E+06	5.88E+06	6.18E+06	6.26E+06	5.92E+06
100ng/ml	3.19E+06	3.06E+06	3.28E+06	3.40E+06	9.62E+05	1.04E+06	1.06E+06	1.01E+06	2.78E+06	2.95E+06	2.87E+06	2.82E+06
1000ng/ml	1.63E+06	1.90E+06	1.76E+06	1.81E+06	5.60E+05	5.86E+05	5.74E+05	5.54E+05	1.53E+06	1.59E+06	1.57E+06	1.58E+06

Supplementary Table 15 related to Figure 9 (B). Quantification of adenosine triphosphate (ATP) to determine resistance of D283 cell line to varying concentrations of vincristine. The results of biological replicate experiments are shown in the tables.

Exp.2	Untreated D283				CCT-8 siRNA				Control siRNA			
Blank	2.33E+03	2.51E+03	2.79E+03	2.63E+03	2.20E+03	1.97E+03	1.95E+03	1.55E+03	2.47E+03	2.53E+03	2.62E+03	2.43E+03
solvent	1.67E+07	1.70E+07	1.73E+07	1.73E+07	1.14E+07	1.15E+07	1.08E+07	1.11E+07	1.56E+07	1.57E+07	1.62E+07	1.59E+07
1ng/ml	1.67E+07	1.76E+07	1.78E+07	1.79E+07	1.01E+07	1.02E+07	9.56E+06	9.60E+06	1.60E+07	1.63E+07	1.66E+07	1.63E+07
5ng/ml	1.54E+07	1.57E+07	1.56E+07	1.52E+07	6.61E+06	6.59E+06	6.61E+06	6.10E+06	1.43E+07	1.45E+07	1.38E+07	1.33E+07
10ng/ml	1.21E+07	1.25E+07	1.26E+07	1.26E+07	4.94E+06	5.21E+06	5.18E+06	5.12E+06	1.12E+07	1.18E+07	1.16E+07	1.13E+07
50ng/ml	7.04E+06	7.00E+06	7.44E+06	7.09E+06	2.58E+06	2.57E+06	2.58E+06	2.48E+06	6.11E+06	6.11E+06	6.28E+06	6.29E+06
100ng/ml	3.22E+06	3.25E+06	3.33E+06	3.38E+06	1.13E+06	1.18E+06	1.11E+06	9.97E+05	3.09E+06	3.12E+06	2.86E+06	2.84E+06
1000ng/ml	1.94E+06	1.86E+06	1.89E+06	1.79E+06	6.45E+05	6.32E+05	6.08E+05	5.57E+05	6.89E+05	1.59E+06	1.63E+06	1.53E+06

Supplementary Table 16 related to Figure 9 (B). Quantification of adenosine triphosphate (ATP) to determine resistance of D283 cell line to varying concentrations of vincristine. The results of biological replicate experiments are shown in the tables.

Exp.3	Untreated D283				CCT-8 siRNA				Control siRNA			
Blank	2.47E+03	2.94E+03	3.23E+03	2.93E+03	2.23E+03	2.13E+03	2.08E+03	1.65E+03	2.59E+03	2.70E+03	2.81E+03	2.56E+03
solvent	1.86E+07	1.91E+07	1.85E+07	1.84E+07	1.23E+07	1.19E+07	1.21E+07	1.22E+07	1.72E+07	1.73E+07	1.70E+07	1.72E+07
1ng/ml	1.85E+07	1.91E+07	1.90E+07	1.85E+07	1.05E+07	1.07E+07	1.09E+07	1.07E+07	1.71E+07	1.74E+07	1.67E+07	1.69E+07
5ng/ml	1.68E+07	1.69E+07	1.66E+07	1.68E+07	6.98E+06	7.11E+06	6.92E+06	6.70E+06	1.53E+07	1.53E+07	1.55E+07	1.49E+07
10ng/ml	1.35E+07	1.35E+07	1.36E+07	1.32E+07	5.38E+06	5.35E+06	5.30E+06	5.42E+06	1.20E+07	1.27E+07	1.25E+07	1.20E+07
50ng/ml	7.53E+06	7.79E+06	7.69E+06	7.68E+06	2.60E+06	2.63E+06	2.50E+06	2.57E+06	6.76E+06	6.70E+06	6.83E+06	6.72E+06
100ng/ml	3.61E+06	3.76E+06	3.74E+06	3.73E+06	1.20E+06	1.18E+06	1.11E+06	1.14E+06	3.35E+06	3.41E+06	3.01E+06	3.21E+06
1000ng/ml	1.93E+06	2.01E+06	1.97E+06	2.03E+06	6.55E+05	7.37E+05	7.35E+05	6.61E+05	1.78E+06	1.88E+06	1.85E+06	1.76E+06

Supplementary Table 17 related to Figure 9 (B). Supplementary Table 15 to 17 related to Figure 6 (B). Quantification of adenosine triphosphate (ATP) to determine resistance of D283 cell line to varying concentrations of vincristine. The results of biological replicate experiments are shown in the tables.

Exp.1	Untreated HD-MB03				CCT-8 siRNA				Control siRNA			
Blank	1.45E+03	1.95E+03	2.05E+03	2.01E+03	1.59E+03	1.56E+03	1.53E+03	1.09E+03	1.95E+03	2.21E+03	2.18E+03	1.97E+03
solvent	1.31E+07	1.32E+07	1.31E+07	1.28E+07	9.68E+06	9.58E+06	9.09E+06	8.83E+06	1.31E+07	1.32E+07	1.31E+07	1.32E+07
1ng/ml	1.34E+07	1.32E+07	1.30E+07	1.26E+07	8.91E+06	8.67E+06	8.87E+06	9.78E+06	1.34E+07	1.36E+07	1.36E+07	1.36E+07
5ng/ml	1.19E+07	1.19E+07	1.16E+07	1.22E+07	8.06E+06	8.24E+06	7.98E+06	7.90E+06	1.14E+07	1.14E+07	1.06E+07	1.04E+07
10ng/ml	9.29E+06	9.54E+06	9.29E+06	9.80E+06	7.28E+06	7.23E+06	6.68E+06	6.79E+06	9.31E+06	8.99E+06	8.20E+06	8.54E+06
50ng/ml	4.56E+06	5.17E+06	4.91E+06	5.13E+06	2.11E+06	1.95E+06	1.80E+06	1.57E+06	4.23E+06	4.26E+06	4.18E+06	3.93E+06
100ng/ml	2.98E+06	3.27E+06	3.25E+06	3.16E+06	8.59E+05	9.14E+05	7.93E+05	7.47E+05	3.09E+06	2.65E+06	2.91E+06	2.70E+06
1000ng/ml	1.85E+05	2.34E+05	2.28E+05	2.15E+05	1.39E+05	1.46E+05	1.39E+05	1.37E+05	2.35E+05	2.71E+05	2.88E+05	2.29E+05

Supplementary Table 18 related to Figure 9 (C). Quantification of adenosine triphosphate (ATP) to determine resistance of HD-MB03 cell line to varying concentrations of vincristine. The results of biological replicate experiments are shown in the tables.

Exp.2	Untreated HD-MB03				CCT-8 siRNA				Control siRNA			
Blank	1.91E+03	2.29E+03	2.39E+03	2.40E+03	2.07E+03	1.96E+03	1.81E+03	1.37E+03	2.51E+03	2.36E+03	2.26E+03	2.09E+03
solvent	1.43E+07	1.54E+07	1.47E+07	1.49E+07	1.14E+07	1.18E+07	1.13E+07	1.13E+07	1.64E+07	1.47E+07	1.50E+07	1.52E+07
1ng/ml	1.43E+07	1.55E+07	1.55E+07	1.53E+07	1.13E+07	1.12E+07	1.14E+07	1.07E+07	1.52E+07	1.52E+07	1.60E+07	1.62E+07
5ng/ml	1.41E+07	1.37E+07	1.41E+07	1.37E+07	9.43E+06	9.39E+06	9.31E+06	8.72E+06	1.28E+07	1.26E+07	1.29E+07	1.25E+07
10ng/ml	1.09E+07	1.10E+07	1.13E+07	1.12E+07	7.74E+06	8.10E+06	7.39E+06	7.45E+06	1.04E+07	1.04E+07	1.03E+07	1.02E+07
50ng/ml	4.98E+06	5.42E+06	5.50E+06	5.21E+06	1.73E+06	1.98E+06	1.88E+06	1.26E+06	4.44E+06	4.50E+06	4.52E+06	4.27E+06
100ng/ml	3.37E+06	3.42E+06	3.55E+06	3.61E+06	8.08E+05	6.85E+05	7.38E+05	6.63E+05	2.86E+06	2.97E+06	2.67E+06	2.82E+06
1000ng/ml	2.32E+05	2.36E+05	2.21E+05	2.11E+05	1.31E+05	1.06E+05	1.13E+05	1.26E+05	1.71E+05	1.67E+05	1.78E+05	1.28E+05

Supplementary Table 19 related to Figure 9 (C). Quantification of adenosine triphosphate (ATP) to determine resistance of HD-MB03 cell line to varying concentrations of vincristine. The results of biological replicate experiments are shown in the tables.

Exp.3	Untreated HD-MB03				CCT-8 siRNA				Control siRNA			
Blank	1.99E+03	2.38E+03	2.31E+03	2.19E+03	1.80E+03	1.72E+03	1.90E+03	1.41E+03	2.00E+03	2.24E+03	2.20E+03	2.11E+03
solvent	1.60E+07	1.53E+07	1.49E+07	1.42E+07	1.11E+07	1.13E+07	1.13E+07	1.13E+07	1.37E+07	1.41E+07	1.44E+07	1.47E+07
1ng/ml	1.47E+07	1.48E+07	1.48E+07	1.45E+07	1.07E+07	1.05E+07	1.08E+07	1.11E+07	1.36E+07	1.40E+07	1.35E+07	1.35E+07
5ng/ml	1.30E+07	1.22E+07	1.24E+07	1.25E+07	8.48E+06	8.49E+06	8.13E+06	9.35E+06	1.23E+07	1.18E+07	1.22E+07	1.19E+07
10ng/ml	9.88E+06	9.73E+06	9.73E+06	9.72E+06	7.44E+06	7.32E+06	7.51E+06	7.49E+06	9.53E+06	9.45E+06	9.49E+06	9.16E+06
50ng/ml	4.71E+06	4.78E+06	4.78E+06	4.89E+06	1.80E+06	1.55E+06	1.24E+06	1.21E+06	4.62E+06	4.32E+06	4.35E+06	4.38E+06
100ng/ml	3.23E+06	3.08E+06	3.33E+06	3.10E+06	6.79E+05	6.98E+05	5.54E+05	4.11E+05	3.04E+06	2.96E+06	2.67E+06	2.78E+06
1000ng/ml	2.43E+05	1.83E+05	2.49E+05	2.63E+05	8.68E+04	1.33E+05	1.20E+05	6.25E+04	1.81E+05	1.72E+05	1.70E+05	1.97E+05

Supplementary Table 20 related to Figure 9 (C). Supplementary Table 18 to 20 related to Figure 6 (C). Quantification of adenosine triphosphate (ATP) to determine resistance of HD-MB03 cell line to varying concentrations of vincristine. The results of biological replicate experiments are shown in the tables.

Exp.1	Untreated D425				CCT-8 siRNA				Control siRNA			
Blank	1.35E+03	1.73E+03	1.66E+03	1.93E+03	1.41E+03	1.52E+03	1.39E+03	1.02E+03	1.50E+03	1.61E+03	1.61E+03	1.29E+03
solvent	9.54E+06	9.89E+06	1.01E+07	9.91E+06	8.48E+06	8.21E+06	7.47E+06	8.15E+06	9.97E+06	9.49E+06	9.61E+06	8.83E+06
1ng/ml	9.80E+06	9.95E+06	1.01E+07	1.02E+07	7.83E+06	7.93E+06	7.87E+06	7.94E+06	9.97E+06	9.37E+06	8.82E+06	8.78E+06
5ng/ml	8.39E+06	8.46E+06	8.43E+06	8.43E+06	6.92E+06	6.97E+06	6.79E+06	6.87E+06	7.91E+06	7.32E+06	7.27E+06	7.18E+06
10ng/ml	7.19E+06	7.06E+06	7.07E+06	7.13E+06	5.12E+06	5.32E+06	5.13E+06	4.93E+06	6.47E+06	6.01E+06	6.18E+06	5.72E+06
50ng/ml	4.85E+06	4.64E+06	4.79E+06	5.27E+06	2.53E+06	2.37E+06	2.46E+06	2.26E+06	4.32E+06	4.16E+06	4.22E+06	3.90E+06
100ng/ml	2.19E+06	2.19E+06	2.08E+06	2.37E+06	1.06E+06	9.80E+05	9.65E+05	9.07E+05	1.67E+06	1.57E+06	1.53E+06	1.54E+06
1000ng/ml	8.11E+05	8.99E+05	8.48E+05	9.79E+05	3.05E+05	3.51E+05	3.20E+05	2.88E+05	6.28E+05	6.01E+05	6.02E+05	6.82E+05

Supplementary Table 21 related to Figure 9 (D). Quantification of adenosine triphosphate (ATP) to determine resistance of D425 cell line to varying concentrations of vincristine. The results of biological replicate experiments are shown in the tables.

Exp.2	Untreated D425				CCT-8 siRNA				Control siRNA			
Blank	1.35E+03	1.45E+03	1.65E+03	1.49E+03	1.48E+03	1.46E+03	1.38E+03	1.08E+03	1.65E+03	1.71E+03	1.52E+03	1.42E+03
solvent	9.21E+06	9.31E+06	9.34E+06	8.97E+06	8.62E+06	8.15E+06	8.00E+06	7.91E+06	9.09E+06	9.04E+06	9.04E+06	8.97E+06
1ng/ml	9.23E+06	9.42E+06	8.91E+06	9.04E+06	8.54E+06	8.37E+06	8.18E+06	7.89E+06	8.81E+06	9.67E+06	9.67E+06	9.00E+06
5ng/ml	8.09E+06	8.29E+06	8.10E+06	8.29E+06	7.08E+06	6.87E+06	6.70E+06	6.64E+06	7.39E+06	7.71E+06	7.70E+06	7.69E+06
10ng/ml	6.97E+06	6.98E+06	6.87E+06	6.71E+06	4.95E+06	5.12E+06	5.04E+06	4.54E+06	6.57E+06	6.33E+06	6.52E+06	6.27E+06
50ng/ml	5.14E+06	5.06E+06	4.73E+06	4.99E+06	2.41E+06	2.35E+06	2.53E+06	2.18E+06	4.65E+06	4.58E+06	4.54E+06	4.37E+06
100ng/ml	2.19E+06	2.24E+06	2.23E+06	2.35E+06	1.14E+06	1.16E+06	1.00E+06	1.08E+06	2.08E+06	2.30E+06	2.21E+06	2.08E+06
1000ng/ml	1.04E+06	9.79E+05	8.90E+05	1.03E+06	3.48E+05	3.41E+05	3.55E+05	3.26E+05	9.00E+05	9.15E+05	8.78E+05	9.28E+05

Supplementary Table 22 related to Figure 9 (D). Quantification of adenosine triphosphate (ATP) to determine resistance of D425 cell line to varying concentrations of vincristine. The results of biological replicate experiments are shown in the tables.

Exp.3	Untreated D425				CCT-8 siRNA				Control siRNA			
Blank	1.20E+03	1.54E+03	1.77E+03	1.65E+03	1.65E+03	1.58E+03	1.47E+03	1.19E+03	1.58E+03	1.54E+03	1.64E+03	1.43E+03
solvent	9.86E+06	9.83E+06	9.83E+06	9.44E+06	9.15E+06	8.73E+06	8.58E+06	8.40E+06	9.41E+06	9.06E+06	9.18E+06	8.92E+06
1ng/ml	9.89E+06	9.89E+06	9.73E+06	9.22E+06	8.98E+06	8.62E+06	8.90E+06	8.17E+06	9.56E+06	8.87E+06	9.49E+06	9.24E+06
5ng/ml	8.22E+06	8.30E+06	8.53E+06	8.56E+06	7.08E+06	7.16E+06	7.03E+06	7.01E+06	7.71E+06	7.86E+06	7.81E+06	8.08E+06
10ng/ml	6.78E+06	6.88E+06	7.13E+06	7.09E+06	5.16E+06	4.92E+06	5.09E+06	4.90E+06	6.20E+06	6.31E+06	6.01E+06	6.10E+06
50ng/ml	4.60E+06	4.89E+06	5.03E+06	4.81E+06	2.54E+06	2.57E+06	2.41E+06	2.25E+06	3.93E+06	4.06E+06	4.22E+06	4.34E+06
100ng/ml	1.95E+06	2.20E+06	2.16E+06	2.28E+06	9.20E+05	1.02E+06	1.05E+06	8.43E+05	1.81E+06	1.63E+06	1.81E+06	1.68E+06
1000ng/ml	8.43E+05	8.26E+05	8.68E+05	9.14E+05	3.39E+05	3.51E+05	3.32E+05	2.49E+05	7.66E+05	6.53E+05	6.26E+05	6.18E+05

Supplementary Table 23 related to Figure 9 (D). Supplementary Table 21 to 23 related to Figure 6 (D). Quantification of adenosine triphosphate (ATP) to determine resistance of D425 cell line to varying concentrations of vincristine. The results of biological replicate experiments are shown in the tables.

11. Declaration of personal contribution

The author contributed to the conception and design of the study, conduction of the experiment, collection of data, and its analysis and interpretation. The author contributed to drafting and revision of the manuscript. The data of MS were made in collaboration with the Proteome Facility at UKE and Ms. Antonia Gocke.

12. Eidesstattliche Versicherung

Ich versichere ausdrücklich, dass ich die Arbeit selbständig und ohne fremde Hilfe, insbesondere ohne entgeltliche Hilfe von Vermittlungs- und Beratungsdiensten, verfasst, andere als die von mir angegebenen Quellen und Hilfsmittel nicht benutzt und die aus den benutzten Werken wörtlich oder inhaltlich entnommenen Stellen einzeln nach Ausgabe (Auflage und Jahr des Erscheinens), Band und Seite des benutzten Werkes kenntlich gemacht habe. Das gilt insbesondere auch für alle Informationen aus Internetquellen.

Soweit beim Verfassen der Dissertation KI-basierte Tools („Chatbots“) verwendet wurden, versichere ich ausdrücklich, den daraus generierten Anteil deutlich kenntlich gemacht zu haben. Die „Stellungnahme des Präsidiums der Deutschen Forschungsgemeinschaft (DFG) zum Einfluss generativer Modelle für die Text- und Bilderstellung auf die Wissenschaften und das Förderhandeln der DFG“ aus September 2023 wurde dabei beachtet.

Ferner versichere ich, dass ich die Dissertation bisher nicht einem Fachvertreter an einer anderen Hochschule zur Überprüfung vorgelegt oder mich anderweitig um Zulassung zur Promotion beworben habe.

Ich erkläre mich damit einverstanden, dass meine Dissertation vom Dekanat der Medizinischen Fakultät mit einer gängigen Software zur Erkennung von Plagiaten überprüft werden kann.

Datum Unterschrift

13. Acknowledgements

First of all, I would like to express my special thanks to the Molecular Neuro-Oncological Pathology research group, the Center for Molecular Neurobiology Hamburg, the University Medical Center Hamburg-Eppendorf. I would like to express my sincere gratitude to all members of the research group for their help in my work.

At the same time, I would like to express my sincere gratitude to my supervisor, Prof. Dr. med. Julia Neumann, for her selfless guidance and care in my studies, work and life. She created conditions for me to coordinate various research groups, which made it possible for me to carry out the necessary research work in their premises. Prof. Dr. med. Julia Neumann's serious academic attitude set an example for students in medicine and scientific research.

In addition, I would like to thank Dr. rer. nat. Nina Struve, a biochemist and medical scientist, of the Laboratory for Radiobiology and Experimental Radio-oncology, and Antonia Gocke, an executive PhD student, of the core facility proteomics, because of their help, my research can become more complete.

Finally, I would like to thank my parents and other family members for their selfless and thoughtful support, which enabled me to devote myself to my studies without any worries.